Tunable hierarchical wrinkling: From models to applications (EP)

Long Ma, Linghui He and (iD) Yong Ni

COLLECTIONS

(EP)   This paper was selected as an Editor's Pick

View Online   Export Citation   CrossMark

ARTICLES YOU MAY BE INTERESTED IN

Hyperbolic metamaterials: From dispersion manipulation to applications
Journal of Applied Physics **127**, 071101 (2020); https://doi.org/10.1063/1.5128679

Engineering of defects in resistive random access memory devices
Journal of Applied Physics **127**, 051101 (2020); https://doi.org/10.1063/1.5136264

Point defects in Ga_2O_3
Journal of Applied Physics **127**, 101101 (2020); https://doi.org/10.1063/1.5142195

Tunable hierarchical wrinkling: From models to applications

View Online   Export Citation   CrossMark

Long Ma, Linghui He, and Yong Ni[a]

AFFILIATIONS

CAS Key Laboratory of Mechanical Behavior and Design of Materials, Department of Modern Mechanics, CAS Center for Excellence in Complex System Mechanics, University of Science and Technology of China, Hefei, Anhui 230026, People's Republic of China

[a]**Author to whom correspondence should be addressed:** yni@ustc.edu.cn

ABSTRACT

Wrinkled surfaces have attracted enormous interest during the past years due to their various wrinkling patterns and impressive multifunctional properties. With the growing demand of numerous potential applications, it is desirable to uncover the formation mechanism and develop fabrication methods for tunable wrinkles, in particular, for hierarchical wrinkle that has spatially varying wavelength and amplitude. In this tutorial, we comprehensively discuss the possible mechanism of the formation of hierarchical wrinkles, including the role of elasticity gradient in film–substrate systems, the effect of boundary confinement, the sequential multistep strain-releasing method in a multilayer system, etc. The formation conditions and morphological features of various hierarchical wrinkling patterns are outlined. Lastly, representative applications of hierarchical wrinkling are briefly summarized as well.

I. INTRODUCTION

Surface wrinkles on compliant substrates are broadly found in natural and biological systems, such as the wrinkle of an aging man's skin, dry fruits, wrinkles of carpets, and even morphologies of folded mountains are considered to be related with the wrinkling phenomenon. When the compression in a substrate-supported film exceeds the criterion, the flat film will lose its stability and wrinkle in various patterns.[1–3] Generally, uniaxial compression leads to unidirectional stripe wrinkles, while biaxial compression may generate chessboard, labyrinth, or herringbone patterns. By introducing compression to the film–substrate system, such as pre-stretch or thermal mismatch, wrinkling patterns are designed and produced controllably, which have been widely used in the thin-film metrology,[4–16] stretchable electronics,[17–25] stretchable functional skins,[26–34] tunable surface wettability,[35–42] functionalized optical devices, like tunable transmittance and light grating,[38–41,43–57] and surface antifouling.[58–60] However, the ordinary wrinkled patterns usually are unidirectional or homogenous and have a uniform wavelength and amplitude for given mechanical properties and applied loading, which severely limit their applications.

Biological materials usually exhibit a complex hierarchical microstructure toward various amazing functions after millions of years of evolution,[61] such as the self-cleaning effect in lotus,[62] robust and releasable adhesion in gecko,[63] remarkable mechanical properties in bone and nacre,[64,65] etc. Therefore, the bioinspired hierarchically structured surface through hierarchical wrinkling is surely believed to broaden the potential and multifunctional applications of wrinkled surfaces beyond uniform surface features, it urgently necessitates us to explore and design a tunable and hierarchical wrinkling pattern. Hierarchical wrinkle is the surface wrinkling that has a spatially distributed wavelength and amplitude and shows a scale hierarchy among the film. Actually, the hierarchical wrinkling phenomena are widely observed in nature. Figure 1(a) shows the translational symmetry breaking of the one-dimensional corrugated profile, which occurs near the edge of an ultrathin polystyrene (PS) sheet floating on fluid.[66] Similar hierarchical wrinkling patterns are also found in hanging curtains and the boundary of the floating thin film or graphene from macro- to micro-length scale.[67–72] In the past few years, the fabrication of hierarchical surface structures by employing mechanical instability of deformable thin materials has attracted much research attention.[38,41,73–76] Figure 1(b) shows an example of the high-resolution picture of the hierarchical nanostructure by a sequential strain-releasing method.[74] This method has showed its outstanding advantages to produce functional
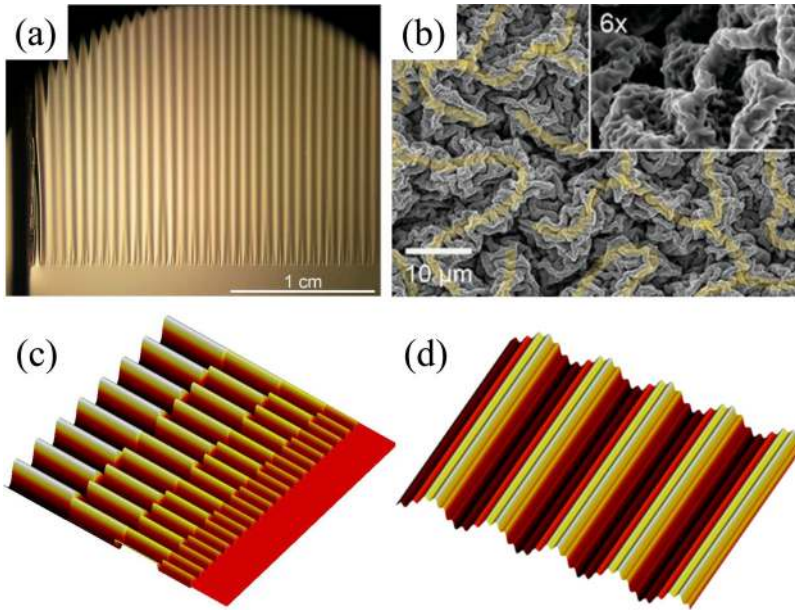
FIG. 1. (a) Hierarchical wrinkle pattern in the floating ultrathin PS film on the surface of water (scale bar is 1 cm and film thickness is 246 nm). Reprinted with permission from Huang *et al.*, Phys. Rev. Lett. **105**, 038302 (2010). Copyright 2010 American Physical Society. (b) Fabricated multigenerational hierarchical nanostructure of a reactive ion etching plasma treated PS substrate by sequential nanowrinkling (scale bar is 10 μm). Reprinted with permission from Lee *et al.*, Nano Lett. **16**, 3774 (2016). Copyright 2016 American Chemical Society. (c) and (d) Schematics of various tunable hierarchical wrinkling patterns.

nanostructures as a bottom-up approach. The researchers aim to design a controllable hierarchical wrinkling surface, such as the tunable and spatially distributed wavelength and amplitude of corrugated morphologies, or the nested wrinkle with several hierarchies, as shown in Figs. 1(c) and 1(d). This tutorial will introduce research progresses on hierarchical wrinkles. First, we will start with the fundamentals of film wrinkling. Then physical mechanisms of ways to generate hierarchical wrinkles are briefly reviewed, including introducing an elastic gradient into the film–substrate system, the effect of boundary confinement, and the artificial sequential wrinkling process. Finally, several potential applications of hierarchical wrinkling are discussed.

II. FUNDAMENTAL OF FILM WRINKLING

First, we review the fundamental concepts of wrinkling patterns.[1,77–85] When a thin film with thickness h and homogenous elasticity on the substrate is under uniaxial compression, one-dimensional wrinkling stripes are generated with wavelength λ and amplitude A, as shown in Fig. 2(a). When the thickness of the substrate is much thicker than the film, the substrate can be regarded as a semi-infinite space and morphological features are only dependent on the film thickness and the elastic modulus of the film–substrate system. The sinusoidal function is employed to describe the out-of-plane displacement $z(x)$ of the deflected film,

$$z(x) = A \sin \frac{2\pi x}{\lambda}. \tag{1}$$

The wavelength of wrinkles is linearly dependent on film thickness h and the amplitude is related to applied compressive strain ε,

$$\lambda = 2\pi h \left(\frac{\bar{E}_f}{3\bar{E}_s}\right)^{\frac{1}{3}}, \tag{2}$$

$$A = h\sqrt{\frac{\varepsilon}{\varepsilon_c} - 1}, \tag{3}$$

where $\bar{E}_f = E_f/(1 - v_f^2)$ and $\bar{E}_s = E_s/(1 - v_s^2)$ are the plane–strain modulus with $E_{f,s}$ and $v_{f,s}$ Young's modulus and Poisson's ratio of the film and the substrate, respectively. Here, ε_c is the critical wrinkling strain that is independent of film thickness and only depends on the modulus ratio,

$$\varepsilon_c = \frac{1}{4}\left(\frac{3\bar{E}_s}{\bar{E}_f}\right)^{\frac{2}{3}}. \tag{4}$$
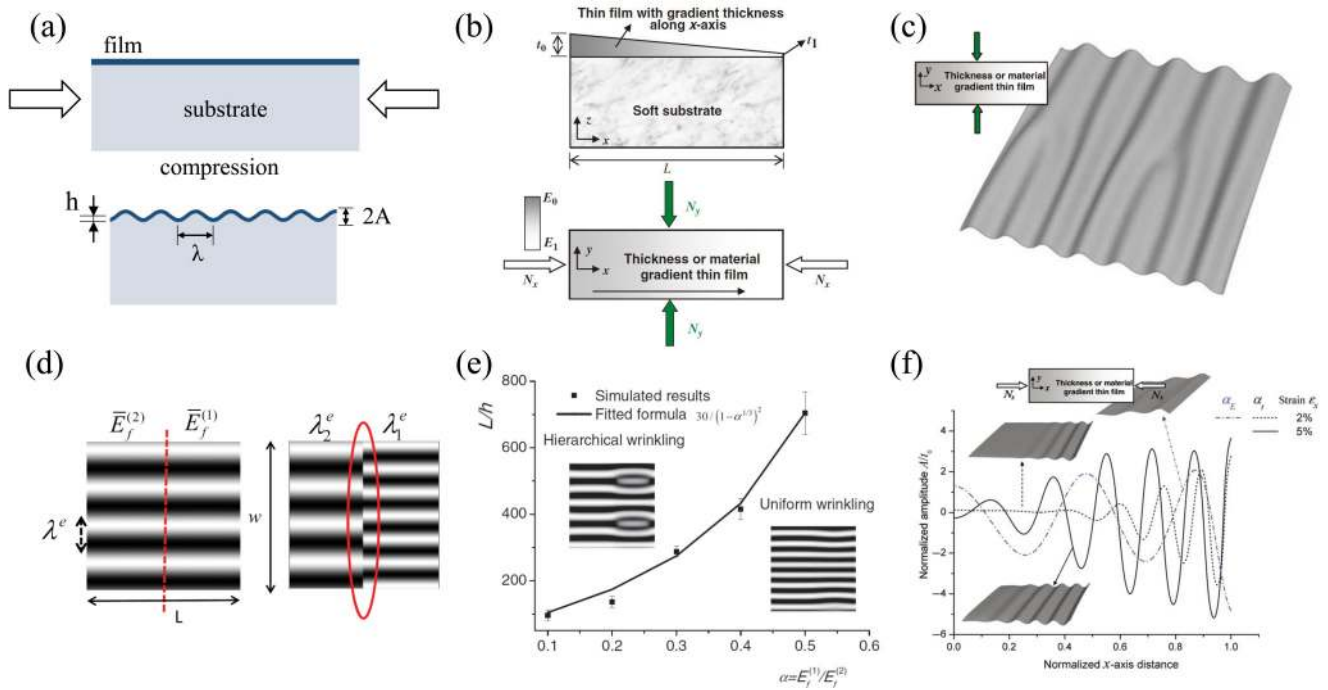
When the film is under biaxial compression, hexagonal, checkerboard, labyrinth, or herringbone wrinkling patterns are produced, whose wavelength λ and amplitude A can also be determined by Eqs. (2)–(4).[78,79,84,86–89]

III. HIERARCHICAL WRINKLING IN ELASTICITY GRADIENT FILM–SUBSTRATE SYSTEM

Limited to uniform thickness and elasticity, films show either parallel stripes or homogenous two-dimensional wrinkling patterns. To overcome this restriction and extend the application of film wrinkling, films with gradient properties both in thickness and in modulus are studied, and the resulted various hierarchical wrinkling morphologies are explored in recent years.

A. Formation mechanism of hierarchical wrinkling due to elasticity gradient

In the beginning, we start with the review of a pioneer work[90] to investigate the wrinkling phenomenon of a gradient film on the complaint substrate. Figure 2(b) shows the schematic of the film system with an elasticity gradient. The film gradient reflects as the

FIG. 2. (a) Formation of uniform wrinkles under uniaxial compression. (b) Schematic of the thin film with gradient thickness or modulus along the x axis on a compliant substrate. (c) Hierarchical wrinkling pattern when the compression is perpendicular to the gradient direction. Reprinted with permission from Yin *et al.*, Philos. Mag. Lett. **90**, 423 (2010). Copyright 2010 Taylor & Francis. (d) Schematic of different wrinkling configurations of a modulus inhomogeneous film system. (e) The relationship between critical branching length and the modulus inhomogeneity. Reprinted with permission from Ni *et al.*, Phys. Rev. E **86**, 031604 (2012). Copyright 2012 American Physical Society. (f) Non-uniform wrinkling pattern when the compression is parallel to the gradient direction. Reprinted with permission from Yin *et al.*, Philos. Mag. Lett. **90**, 423 (2010). Copyright 2010 Taylor & Francis.

film thickness gradient $t(x)$ or Young's modulus gradient $E(x)$ and $t(x)$ or $E(x)$ are assumed linearly dependent on the location in the x direction,

$$t(x) = t_0(1 - \alpha_t x/L) \quad \text{or} \quad E(x) = E_0(1 - \alpha_E x/L), \quad (5)$$

where L is the length of the film along the x direction, t_0 and E_0 are the thickness and Young's modulus of the film at $x = 0$, respectively, and $0 < \alpha_t, \alpha_E < 1$ are the coefficients that character the elasticity gradient. Then, $t_1 = t_0(1 - \alpha_t)$ and $E_1 = E_0(1 - \alpha_E)$ are the thickness and Young's modulus of the film at $x = L$, respectively, as shown in Fig. 2(b).

The wrinkling of the gradient film is studied under uniaxial compression that is perpendicular or parallel to the gradient direction separately. When the compression direction is perpendicular to the gradient direction, which means applying force N_y along y axial on the film in Fig. 2(b), the Finite Element Model (FEM) results show that compression generates Y-branched wrinkle pattern as in Fig. 2(c).[90] In the film with uniform thickness and modulus, wrinkle stripes are generally parallel-arranged and perpendicular to the direction of compression. In the gradient film, compared with uniform one-dimensional wrinkle stripes, the branched wrinkle pattern is inhomogeneous both in wavelength

and amplitude along the gradient direction. At the thicker region, the film has a large wavelength and amplitude, while at the thinner region they are both smaller. There is a transition zone in the film between different wavelengths that present a Y-shaped junction and forms a hierarchical wrinkling pattern as shown in Fig. 2(c).

According to Eqs. (2) and (3), the wavelength and amplitude are proportional to the film thickness, so it is easy to accept that the gradient film has different wavelengths and amplitudes with varying thickness or modulus. However, will the hierarchical structure always show up whenever the elasticity gradient exist? The answer is no based on the discussion below. To understand the steplike variation of the wavelength with respect to the film thickness, and the critical stiffness gradient or the critical characteristic length of stiffness inhomogeneous film for the formation of a hierarchical and branched wrinkling pattern, it requires to take into account the total elastic energy of the film system with elastic inhomogeneity. When the unidirectional wrinkling pattern is under the approximation of the sinusoidal form, the shear stress at the interface between the film and the substrate is negligible, and the total elastic energy of the homogeneous film–substrate system includes the bending energy U_b^{film}, the stretching energy U_s^{film} of the film, and the elastic energy U^{sub} of substrate.[87] For the given out-of-plane deflection Eq. (1) with wavelength λ and amplitude A,

the total elastic energy per unit area U in the wrinkled film can be expressed as[87,91]

$$\frac{U}{U_0} = 1 - \left[1 - \left(\frac{\pi^2 h^2}{3\lambda^2} + \frac{\lambda \bar{E}_s}{4\pi h \bar{E}_f} \right) / \varepsilon_{pre} \right]^2,$$ (6)

where $U_0 = \frac{1}{2} h \bar{E}_f \varepsilon_{pre}^2$ with ε_{pre} the uniaxial compression. Equation (6) means that for the given modulus ratio $\bar{E}_f^{(1)}/\bar{E}_s$, the system has a minimum total energy at a specific equilibrium wavelength of $\lambda_1^e = 2\pi h (\bar{E}_f^{(1)}/3\bar{E}_s)^{\frac{1}{3}}$ when ε_{pre} exceeds critical wrinkling strain $\varepsilon_c^{(1)} = \frac{1}{4}(3\bar{E}_s/\bar{E}_f^{(1)})^{\frac{2}{3}}$. In the same way, the system with different modulus ratios $\bar{E}_f^{(2)}/\bar{E}_s$ has another equilibrium wavelength λ_2^e. Then, a system with inhomogeneous film moduli $\bar{E}_f^{(1)}$ and $\bar{E}_f^{(2)}$ at two sides is considered.[91] Figure 2(d) shows two hypothetic wrinkling morphologies of the inhomogeneous system. The left means that the wrinkled stripes are coherent and have an intermediate wavelength $\lambda_1^e < \lambda^e < \lambda_2^e$, while the right configuration shows that there is a dislocated boundary between two wavelengths λ_1^e and λ_2^e, which corresponds to equilibrium wavelengths of film moduli $\bar{E}_f^{(1)}$ and $\bar{E}_f^{(2)}$, respectively. The energy changes of these two configurations in Fig. 2(d) with respect to the case of uniform modulus are expressed as $\Delta U L w$ in the uniform wrinkle and $\gamma_l w$ in the dislocated wrinkle, where $\Delta U = U(\lambda^e)$; γ_l is the effective line energy at the dislocated boundary; and L and w are the size of the wrinkle, respectively. To decide which configuration is energetically favorable, a coherency persistent length $L_c = \gamma_l / \Delta U$ is defined. Ni et al. proposed that the branched wrinkling system can be made an analogy with the two separated phases with a boundary. By employing Gibbs's description and the classic diffuse interface theory,[92] the coherency length of the branched wrinkle can be approximately obtained as

$$L_c = \frac{C}{(1 - \alpha^{1/3})^2},$$ (7)

where $\alpha = \bar{E}_f^{(1)}/\bar{E}_f^{(2)} (\bar{E}_f^{(1)} \leq \bar{E}_f^{(2)})$ is the modulus ratio of the inhomogeneous film and $C \approx \sqrt{\beta/B}(3\bar{E}_s/\bar{E}_f^{(2)})^{1/3}/(2\pi h)^2$ is a constant with β and B the assumed invariants. If the characteristic length of the modulus inhomogeneous exceeds the critical length $L > L_c$, the film wrinkling loses its coherency and a branched hierarchical wrinkled pattern appears. Figure 2(e) shows the relationship between elastic inhomogeneous and the critical branching length, in which scatters are calculated by solving the Föppl–von Kármán (FvK) plate equation using the gradient-flow method, and the line is fitted by the formula in Eq. (7). The results demonstrate that for a given characteristic length, the hierarchy of the wrinkling pattern only appears when stiffness inhomogeneous exceeds a critical value, and the critical characteristic length for the hierarchical wrinkle increases with the increase of stiffness inhomogeneous.

When compression is parallel to the direction of film thickness or stiffness gradient, parallel wrinkles that are perpendicular to compression are generated. The FEM results[90] show that the wrinkles first emerge at the thinnest or the most complaint region of the film and then gradually propagate to the whole film. This phenomenon can be understood that the thinner or more complaint region would reach the criterion of wrinkling earlier according to Eq. (4). The wrinkling profiles in Fig. 2(d) show that the wavelength and amplitude are both non-uniform and position-dependent, in which the wavelength increases with the increase in film thickness/stiffness, while the amplitude possesses the opposite tendency. Due to remarkable nonlinearity of the wrinkled profile, it is difficult to find an analytical solution to describe the out-of-plane displacement even under simplified assumptions. Even though, the mode of out-of-place displacement can be fitted as[90]

$$z_0(x) = A(1 + \alpha \pi \bar{x}) \sin(m\pi \bar{x}(1 + \alpha \pi \bar{x})),$$ (8)

where $\bar{x} = x/L$ is the normalized position with L the length of the wrinkled sample, α characters the gradient, and A and m are the effective amplitude and effective wave number that character the wrinkle shape, respectively. Numerical results show that the effective wavelength, effective amplitude, and the critical wrinkling force all depend on the film gradient. If the stiffness of the substrate is gradient and position-dependent, the numerical results from FEM show that the non-uniform wrinkle has an analogous shape that depends on both the absolute value and the gradient of the substrate stiffness.[93]

In common cases, like thermal expansion mismatch during film deposition, or solvent diffusion induced isotropic swelling, the biaxial compression can also be exerted onto film–substrate systems. To study the wrinkling pattern of the gradient film under biaxial compression, thickness-gradient metal nickel (Ni) films are deposited on a polydimethylsiloxane (PDMS) substrate by magnetron sputtering technique, and residual biaxial compression due to isotropic thermal expansion mismatch is exerted.[94] Atomic force microscopy (AFM) images show that biaxial compression generates ordered hierarchical wrinkling patterns in the gradient film. Parallel stripes, herringbones, and labyrinths are observed adjacently in one gradient sample. With the change in film thickness gradients, distributions of ordered wrinkling patterns can be regulated, which draws promising applications in tunable optical or microfluidic templates. The complex wrinkling pattern can be regarded as the superposition of two kinds of patterns under uniaxial compression, which is perpendicular and parallel to the gradient direction, as shown in numerical results [Figs. 3(a)–3(d)]. Figure 3(a) shows the sketch for the superposition of the thickness-gradient film under biaxial compression. The numerical result in Fig. 3(b) shows the branched wrinkles when the compression is perpendicular to the film gradient direction, whose wavelength and amplitude both decrease along the direction of decreasing thickness. Figure 3(c) shows straight wrinkle stripes perpendicular to the gradient direction when the loading is parallel to the gradient direction. The wrinkles in Fig. 3(c) are distributed locally and are absent in the thickest region, in accordance with the result in Fig. 2(f). Figure 3(d) shows the case when the gradient film is under biaxial compression. It can be found that in the thickest region, only the parallel wrinkle stripes in Fig. 3(b) contribute to the superposition. With the decrease in film thickness, the parallel stripes in Fig. 3(c) come into play but the branched stripes in Fig. 3(b) still dominate, thus herringbones form in Fig. 3(d). When the film thickness continues to decrease, the wrinkles that are perpendicular to the gradient direction become comparable to the wrinkles that are parallel to the gradient direction, so there is a
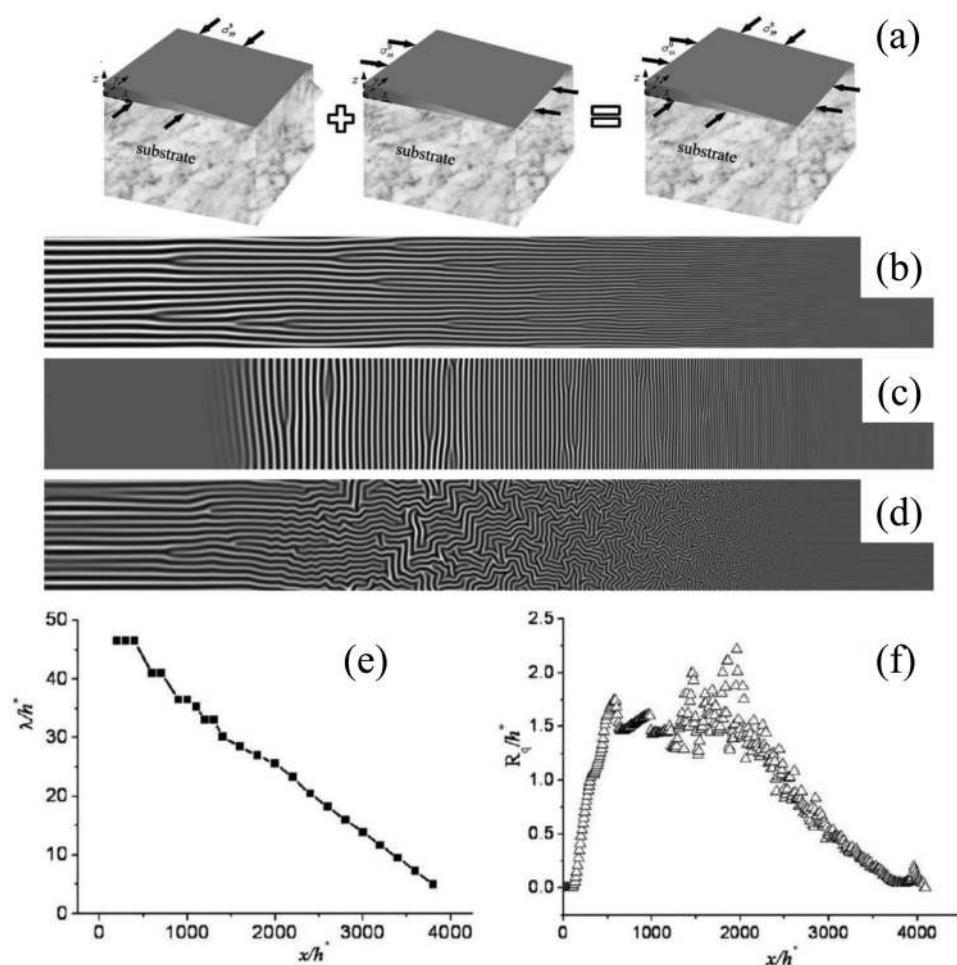
FIG. 3. (a) Sketch of the thickness-gradient film under biaxial compression understood as the superposition of the thickness-gradient film under two orthogonal uniaxial loading directions. (b) and (c) Simulated wrinkling patterns of the thickness-gradient film under uniaxial compression that are perpendicular and parallel to the gradient direction, respectively. (d) Simulated wrinkling pattern of the thickness-gradient film under biaxial compression. (e) and (f) The relationship between normalized average short wavelength and average root square deflection amplitude of hierarchical wrinkling patterns in Fig. 3(d) with respect to normalized distance x with h^* the film thickness, respectively. Reprinted with permission from Yu *et al.*, ACS Appl. Mater. Interfaces **7**, 5160 (2015). Copyright 2015 American Chemical Society.

relatively large region in Fig. 3(d), which is covered by labyrinthlike wrinkles. Although the superposition of two orthogonal loading directions can give a brief description of the ordered hierarchical wrinkling under biaxial loading, it should be noted that the deformation of the thin film cannot be additive due to nonlinearity. Researchers also investigate the statistical morphological characteristic of hierarchical wrinkles under biaxial compression. Figure 3(e) shows that the average wavelength of hierarchical wrinkling is found to decrease with the decrease in film thickness, which is in accordance with the relationship in Eq. (2). However, the average root square deflection amplitude in Figs. 3(f) first increases and then decreases with decreasing film thickness, which differs from that in the uniaxial compressed system.[90]

B. Experimental methods to fabricate elasticity gradient film–substrate systems

Hereinbefore, the numerical simulated results show various wrinkling morphologies of the elasticity gradient film under different loading directions, and the theoretic analysis gives a

characteristic length for the branched hierarchical wrinkles. These results provide the basic guidance for the wrinkling phenomenon in film–substrate systems with elasticity gradient. Here, we outline several experimental methods for fabricating the elasticity gradient film system, mainly including film thickness gradient and substrate stiffness gradient.

First, we review the fabrication of a thickness-gradient film on a soft substrate. A common method to fabricate the wrinkling surface is microfolding due to shrinkage effects after the surface modification of a soft polymer, like PDMS, is under plasma ultraviolet-ozone (UV/O) treatment.[53,74,79,95–108] When the stretching polymer is under UV/O treatment, the UV cured top surface of the substrate becomes a rigid oxide layer. Due to pre-stretching or the shrinkage effect of the polymer, the release of the strain after UV/O treatment then creates a wrinkling pattern due to the stiffness mismatch between the top stiff layer and the soft substrate when the strain exceeds the critical wrinkling strain. It has been already depicted that the modulus and the thickness of the silica layer on the top of the PDMS surface can be tuned by the exposure time,[79,109–111] so the film–substrate system with gradient film

thickness can be easily fabricated. For example, to create a film with continuously varying thickness, a shielded plasma oxidation is conducted by using a triangular prism mask to regulate the exposure time of different regions of the PDMS surface.[112] The thickness-gradient film can also be fabricated by tuning the distance between the UV lamp and the PDMS sample.[113] In brief, the gradient film thickness can be produced by the gradient UV/O treatment, as illustrated in Fig. 4(a).

Besides the continuously changed film thickness, the film thickness can also be modulated as stepwise gradient as shown in Fig. 4(b). The masks like glass plates are used to block specific regions of the PDMS substrate during UV/O treatment, and the sequential change of the masks location can modulate the plasma dose and produce a film with varying thickness in different regions.[114] The discontinuous film thickness not only generates hierarchical wrinkles that have different wavelengths and amplitudes in different regions, but also creates thickness steps in adjacent regions, which can even tune mechanical properties of 2D materials at the nanoscale.[115] The property of polymer resin can also be utilized to produce thickness-gradient film. Patterned PDMS substrates with parallel grooves are prepared by soft-lithography to act as supporters and provide physical boundaries. Polymer resin is then spin-coated on the patterned substrate and the grooves are filled with meniscus surfaces due to surface tension of flowing resin. Then, the thickness-gradient film that is separated by edges of the patterned substrate is fabricated after plasma treatment, as shown in Fig. 4(c). The film is thickest near the edges and thinnest at the middle. The edges also play the role of boundary confinement and create uniaxial compression parallel to the edges, so hierarchical wrinkles perpendicular to the edges form on a patterned substrate.[116] Figure 4(d) shows the sketch of preparing the thickness-gradient film by a flow-coating method. An angled steel blade is used to spread a drop of polymer solution on the substrate. By automatically controlling the moving speed of the blade in a constant acceleration, the solution is distributed non-uniformly on

the substrate and a polymer film with thickness-gradient forms due to drying of solvent within several seconds.[4,117,118]

The metal thin films on the soft substrates are another important system besides the UV/O treated PDMS. Generally, the metal films are deposited on the soft substrate by means of vapor evaporation or sputter deposition, and the film thickness can be directly controlled by the deposition time. To deposit a metal film with thickness gradient on a PDMS substrate, a steel shutter is placed between the substrate and the metal target during the direct current (DC) magnetron sputtering as shown in Fig. 4(e). Due to diffusion of gas particles, some of metal atoms can deposit underneath the shutter. So the thickness of the deposited film is non-uniform on the substrate, and the subsequent investigation shows that the thickness of the metal film has approximately linear relationship with the location. In this method, the maximum and gradient of the film thickness can be regulated by the deposition time and the distance between the shutter and substrate, respectively.[94] Recently, the fixed shutter is replaced by a computer-controlled shutter mask, whose closing speed is adjustable to monitor the film thickness by quartz crystal microbalances.[119]

In addition to the film thickness gradient, many efforts have been made to change the substrate stiffness in film wrinkling systems, mostly in soft PDMS substrates.[100] There are mainly two strategies to prepare the PDMS substrate with stiffness gradient, controlling the PDMS components and controlling the PDMS curing temperature. Claussen et al.[120,121] first created compositional gradient PDMS using a precision syringe pump setup. The hard and soft PDMS components are integrated in a gradient PDMS specimen that is then embedded into a hard PDMS matrix and cured. The wrinkling with continuously changed wavelength is then observed in the stiffness-gradient substrate as illustrated in Fig. 4(f). Furthermore, when the gradient specimen is embedded into the hard matrix, it creates a sharp interface of mechanical properties between different PDMS phases. At the interface of hard and soft components, the wrinkle stripes would bifurcate,
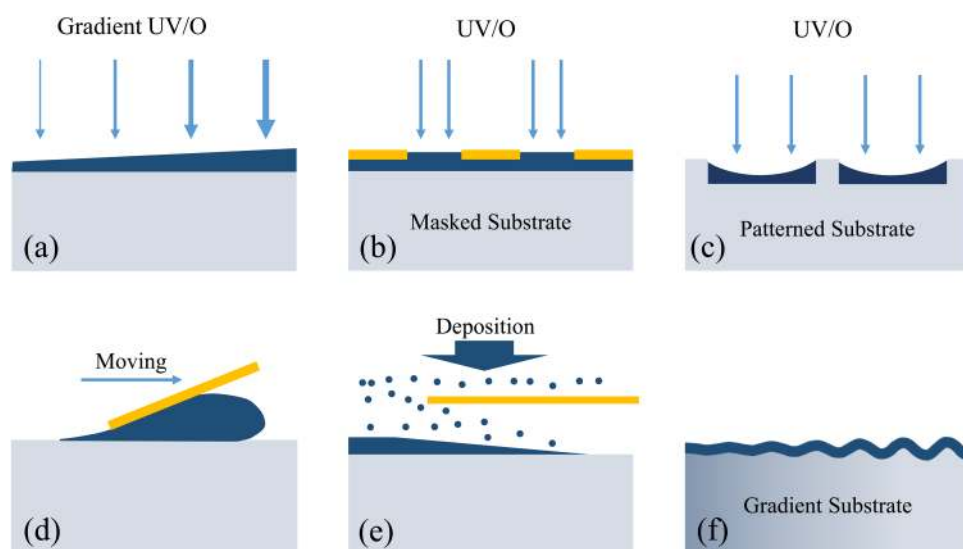
FIG. 4. Schematic diagram of methods to generate elasticity gradient in the film–substrate system. (a) The gradient UV/O treatment. (b) Masking substrate during the UV/O treatment. (c) Using a pre-patterned substrate. (d) Flow-coating method using a moving blade. (e) Using a shield shutter during film deposition. (f) Preparing a stiffness-gradient substrate by controlling components and curing temperature.

forming dislocation-like defects and hierarchical wrinkling patterns.[122]

It has been studied that the mechanical properties of PDMS especially the elastic modulus strongly depend on the curing temperature and the curing time.[123] By applying the temperature gradient during the curing process of liquid PDMS, stiffness-gradient PDMS substrate can also be obtained. In experiments, to provide a gradient temperature field, the PDMS sample is placed on a hot supporter at one side and a cold supporter at another side. The cross-link degree of the elastomer varies with the spatial temperature gradient, and the PDMS elasticity increases with the curing temperature increases.[124–127] It is worth noting that the gradient PDMS sample could even be liquid or viscous state at the cold side and purely elastic state at the hot side. Thus, there exists a transition from surface folds to wrinkles on this kind of gradient sample due to the thermal expansion mismatch after the deposition of the metal film,[125] showing different wrinkling morphologies on one PDMS sample.

C. The elasticity gradient due to diffusion and visco-elasticity effect

The pre-prepared film–substrate system with gradient elasticity provides excellent platform for the fabrication of hierarchical wrinkles with branching structure and varying wavelength and amplitude. For the initially homogeneous elastic system, the hierarchical wrinkling pattern can also be created in virtue of the diffusion and visco-elasticity effect.[91,128,129] At the beginning, we briefly review the mechanism of the diffusion coupled surface wrinkling. Generally, for the system of thin titanium (Ti) layers on the polystyrene (PS) and silicon oxide (SiO$_x$) substrate (Ti/PS/SiO$_x$ multilayer),[130] the thermal expansion mismatch during metal deposition cannot reach the critical wrinkling stress in Eq. (4) due to the relatively large modulus of PS. Thus, surface instability will not be triggered in Ti/PS/SiO$_x$ multilayers and the thin film remains flat after thermal deposition, which differs from the multilayers made up of low modulus elastomers like PDMS,[78] or the cases when the applied stress is larger than the critical stress.[1,87,131] However, the Ti film is still under compression and ready to wrinkle once the ambience changes. When the multilayer sample is put in toluene vapor, the PS would experience a sharp fall of the elastic modulus as well as glass transition temperature during the diffusion of solvent vapor due to sensitivity of the polymer layer to chemical stimulation. Once the modulus of the PS substrate decreases dramatically, the stored stress in the metal thin film can easily exceed the new critical wrinkling stress that strongly depends on the substrate modulus. Thus, the diffusion of solvent can trigger wrinkling formation and determine morphology of the wrinkling pattern. During the diffusion process, wrinkles closely following the diffusion front with the orientation perpendicular to the front. Usually the wrinkles are parallel or radial stripes, which extend from the film edge or pointlike defect, respectively.[10,130,132]

When the PS layer is made up of small chains, the PS becomes viscous during solvent diffusion.[128] It is known that the surface wrinkle undergoes a coarsening process on a viscoelastic substrate.[85,133–136] During the coarsening process, the wrinkle wavelength increases with the decrease in substrate stiffness due to

stress-driven viscoelastic relaxation. The wavelength is also time-dependent. A scale analysis gives that the wavelength for the multilayers has the relationship of[128]

$$\lambda \sim (hH_p)^{1/2}(E/\eta)^{1/6}t^{1/6}, \qquad (9)$$

where h and H_p are the thicknesses of metal and polymer layers, respectively; E is the modulus of the metal film; η is the polymer viscosity; and t is time. The diffusion induced reduction of the substrate modulus together with the viscoelastic effect produces both spatially and temporally dependent wrinkle propagation. Figure 5(a) shows sequential images of wrinkle propagation by diffusion and viscoelastic effects of Ti/PS/SiO$_x$ multilayers in toluene vapors. The parallel wrinkling stripes move with the diffusion front from an edge at first. With the substrate becomes viscoelastic, the already formed wrinkles coarsen, which leads to cascade branched and hierarchical wrinkles. For the diffusion process, the distance from the diffusion front y has the scale of $y \sim t^{1/2}$. Combining with the relationship in Eq. (9) that $\lambda \sim t^{1/6}$, the wavelength of the hierarchical wrinkle in Fig. 5(a) then scales as $\lambda \sim y^{1/3}$, in agreement with experiments.[128] Figures 5(b) and 5(c) show radial hierarchical wrinkling patterns. On the basis of numerical simulation on wrinkle formation due to solvent diffusion mediated inhomogeneous swelling,[137] Ni considered viscous flow and developed the numerical method to reproduce the hierarchical film wrinkles on the substrate whose stiffness gradient is dynamically changed.[91] Figures 5(d) and 5(e) show the simulated wrinkle morphologies of parallel branching stripes and radial wrinkles due to the viscoelastic effect, respectively.

IV. HIERARCHICAL WRINKLING INDUCED BY BOUNDARY CONFINEMENT

In a film–substrate system, the boundary condition plays an important role in the deformation under different loadings. Here, we briefly review the effects of two types of boundary confinement on the formation of hierarchical wrinkling: the bonding interface between the film and the substrate, and the edge of the film. Generally, the interface between the film and the substrate is regarded as homogeneous, and the film is perfectly attached to the substrate. If the interface is relatively weak, the film may delaminate from the substrate and form a buckle-delamination structure directly on the hard substrate[11,138–142] or experience a transition from wrinkling to buckle-delamination on the soft substrate.[143] In the presence of interfacial sliding, the critical buckling stress and equilibrium morphology of film buckling are different from the case when the interface is well attached.[142,144–147] For the substrate with discrepant slippery and sticky domains, the wrinkling pattern shows spatial distribution related to interface properties.[131] When the film is under compression, the displacement in the substrate depends on the boundary constraint and is different in slippery or sticky regions, leading to different equilibrium wavelengths and critical wrinkling strain according to energy minimization. By regulating the adhesive property of interface, the hierarchical wrinkling pattern with different orientations, which are parallel to the boundary in slippery domains and perpendicular to the boundary in
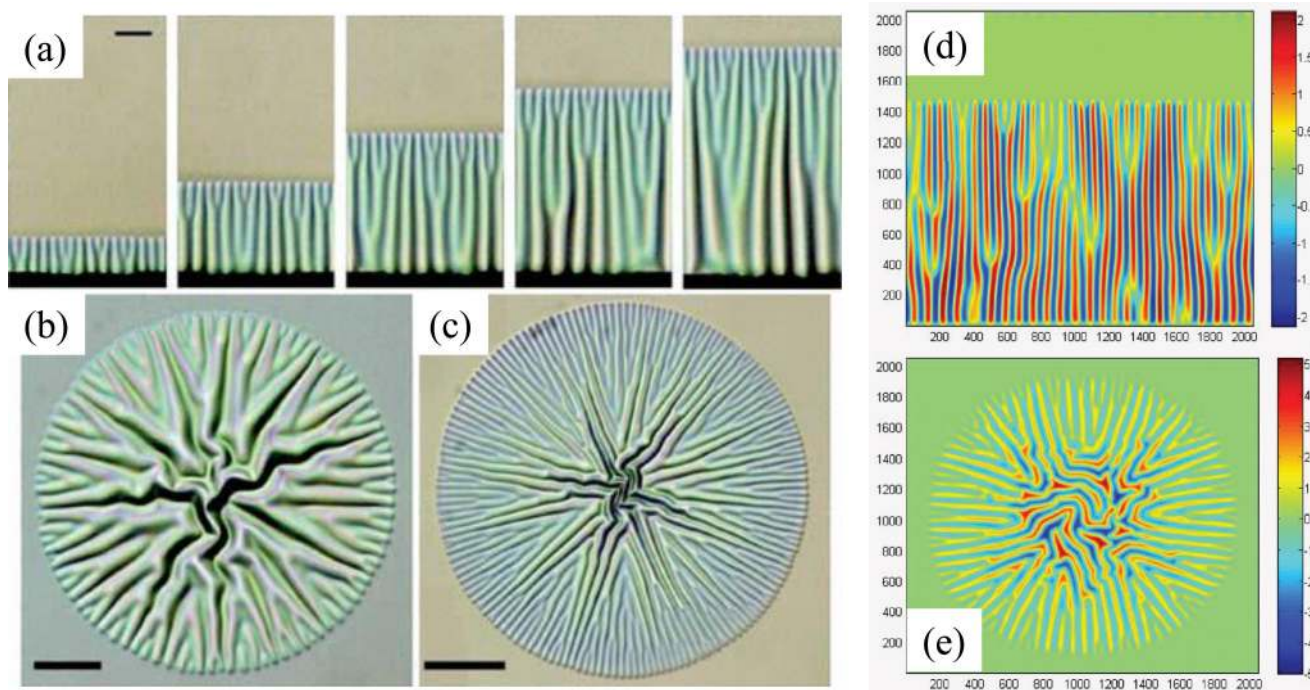
FIG. 5. (a)–(c) Sequential optical images of a branched wrinkling pattern triggered by solvent diffusion and the viscoelastic effect of a Ti/PS/SiOx multilayer after immersion in toluene vapors (scale bar 10 mm). Reprinted with permission from Vandeparre et al., Soft Matter **6**, 5051 (2010). Copyright 2010 Royal Society of Chemistry. (d) and (e) Simulated results of visco-elasticity mediated hierarchical wrinkles (The length scale in the simulation is normalized by top layer thickness h with h = 1.). Reprinted with permission from Ni et al., Phys. Rev. E **86**, 031604 (2012). Copyright 2012 American Physical Society.

sticky domains, and different amplitude, which is larger in slippery domains than that in sticky domains, are obtained.

Near the film edge there usually exists some other physical effects that govern the wrinkling pattern. When an ultrathin PS film floats on water, the translational symmetry breaks and cascaded wrinkles form at the edge of the film.[66] The competition between gravity of the liquid surface, bending energy of the thin film, and capillarity at the boundary creates three characteristic lengths and dominates the morphology of film wrinkling. Similar hierarchical wrinkles with continuously varying wavelength from the edge to interior of the film are also found in metal films deposited on contracting liquid drops like silicone oil drops.[71,148] In this case, an energy analysis that considers bending energy, gravitational energy, thermal expansion, and the surface energy induced by capillarity can obtain well description of the wavelength change at the edge of the film. Recently, a work studies the spontaneous formation of oscillatory cracks and hierarchical wrinkles of metal films on liquid stripes.[72] The wrinkling has a labyrinth pattern at the center of stripe and a hierarchical structure with changing wavelength near the stripe edge. Together with wavy cracks confined in stripes, this study shows various failure modes in constrained film structures.

From the suspended graphene to hanging curtains, the hierarchical wrinkling structures induced by boundary confinement exist widely in constrained thin film, as shown in Figs. 6(a) and 6(b),

respectively. It is found that the wavelength λ that reflects the wrinkling hierarchy has a simple power law with the distance to the edge x among various materials: $\lambda \sim x^n$, which is in accordance with previous theoretical assumptions.[68,149,150] The power exponent n is robust and nearly equals to 2/3 for "light" sheets, like short fabric and paper sheets, and 1/2 for "heavy" sheets, like long fabric, rubber curtains, and constrained graphene. To provide a better understanding of the universal self-similar wrinkling hierarchy by boundary constraint, a formalism is established based on the geometry constraint and energy scaling.[69] The bending and stretching energy of the thin film in a characteristic area $L\lambda$ are considered, where λ is the wavelength and L is the distance in which the wavelength branches into its double. For the sinusoidal deformation with amplitude A, the effective lateral compression induced by edge confinement scales as $\Delta \sim (A/\lambda)^2$ according to the inextensibility hypothesis. With the curvature of out-of-plane undulations $\kappa \sim A/\lambda^2$, the bending energy of the thin sheet in the characteristic area can be expressed as $U_B \sim Eh^3\kappa^2(L\lambda) \sim Eh^3\Delta L\lambda^{-1}$ with film thickness h. The effective elongation strain has the order of $(A/L)^2 \sim \lambda^2\Delta/L^2$, with A/L the average slope of the membrane so the stretching energy can be estimated as $U_s \sim Eh(\lambda^2\Delta/L^2)^2(L\lambda) \sim Eh\lambda^5\Delta^2 L^{-3}$. By minimizing the total energy $U_{tot} = U_B + U_S$ in the characteristic area $L\lambda$ with respect to the transition length L, the optimal characteristic length can be obtained as $L(\lambda) \sim \Delta^{1/4}\lambda^{3/2}h^{-1/2}$. Reminding the geometric constraint that $d\lambda/dx = \lambda/L$, the relationship between the
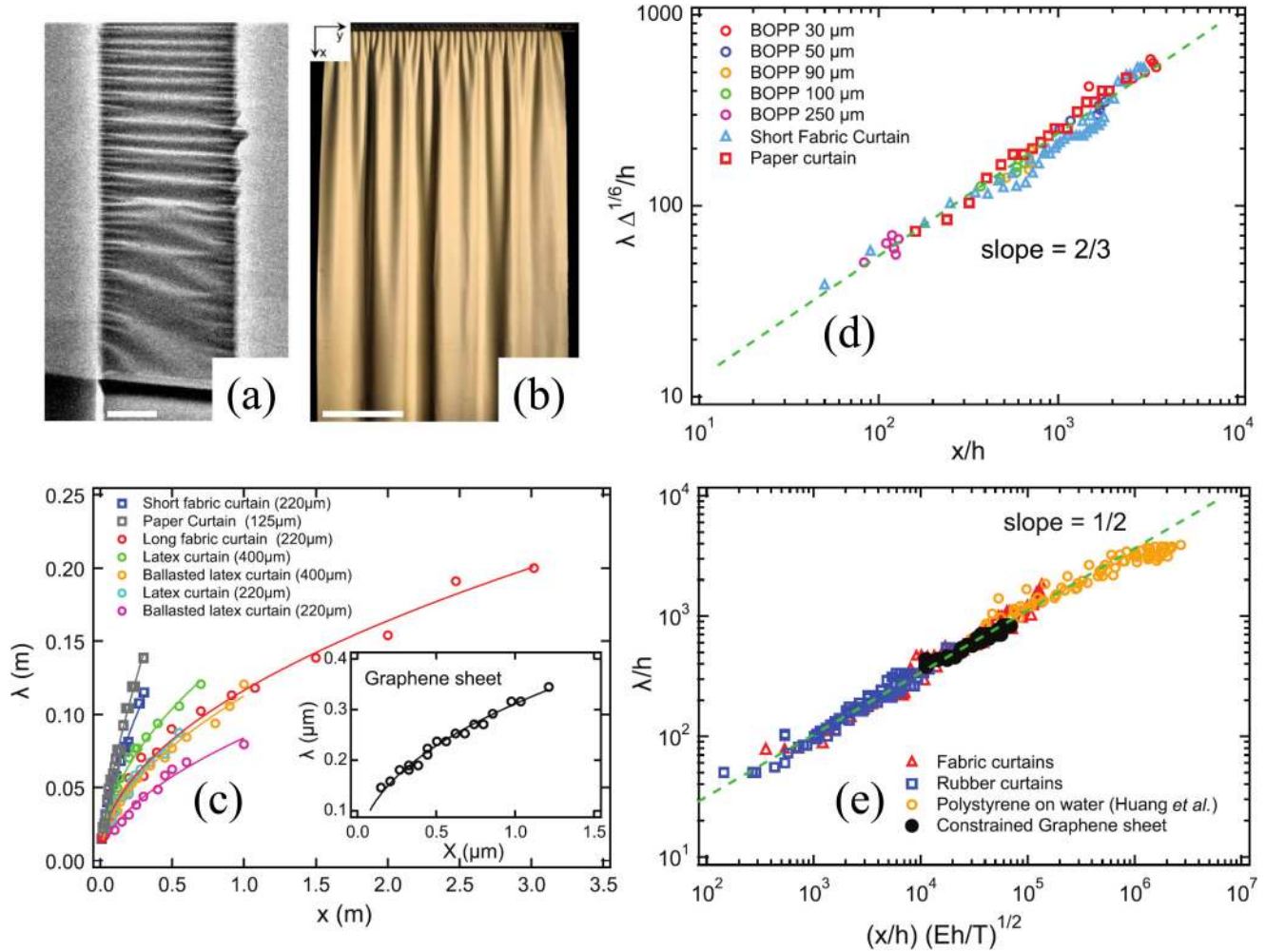
FIG. 6. (a) and (b) Hierarchical wrinkling patterns in a suspended graphene bilayer and a rubber curtain, respectively [scale bars are 1 μm in (a) and 25 cm in (b), respectively]. (c) The power law fits between the wavelength and the distance from the film constrained edge for various curtains. The inset graph shows the relationship between the wavelength and the distance from the constrained edge for a graphene sheet. (d) and (e) The relationship between the normalized wavelength and the normalized distance from the constrained edge for "light" sheets and "heavy" sheets, respectively. Reprinted with permission from Vandeparre et al., Phys. Rev. Lett. **106**, 224301 (2011). Copyright 2011 American Physical Society.

normalized wavelength and location can be obtained as

$$\lambda(x)\Delta^{1/6}/h \sim (x/h)^{2/3}, \tag{10}$$

which is in good agreement with the experimental data for short "light" sheets in Fig. 6(d).

For heavy sheets, there is an additional tensile force imposed on sheets, like the gravity for heavy curtains, the tensile strain by thermal treatment for graphene sheets,[151] and the surface tension or thermal expansion near the edge of the thin film on liquid drops.[66,71,72,148] The stretching energy $U_T \sim T(A/L)^2(L\lambda) \sim T\Delta\lambda^3 L^{-1}$ induced by the tensile stress T takes the dominant place of U_S, and the minimization

of total energy $U_{tot} = U_B + U_T$ leads to $L(\lambda) \sim \lambda^2/h\sqrt{T/Eh}$. So for "heavy" sheets, the wavelength changing with location in the relation of

$$\lambda(x)/h \sim (Eh/T)^{1/4}(x/h)^{1/2}, \tag{11}$$

which is consistent with the experimental results as shown in Fig. 6(e). The boundary confinements provide the geometric constrain and excess tensile stress to compete with the bending energy that always prefers large wavelength, and the competition between bending energy and stretching energy leads to the hierarchy of wrinkling patterns.
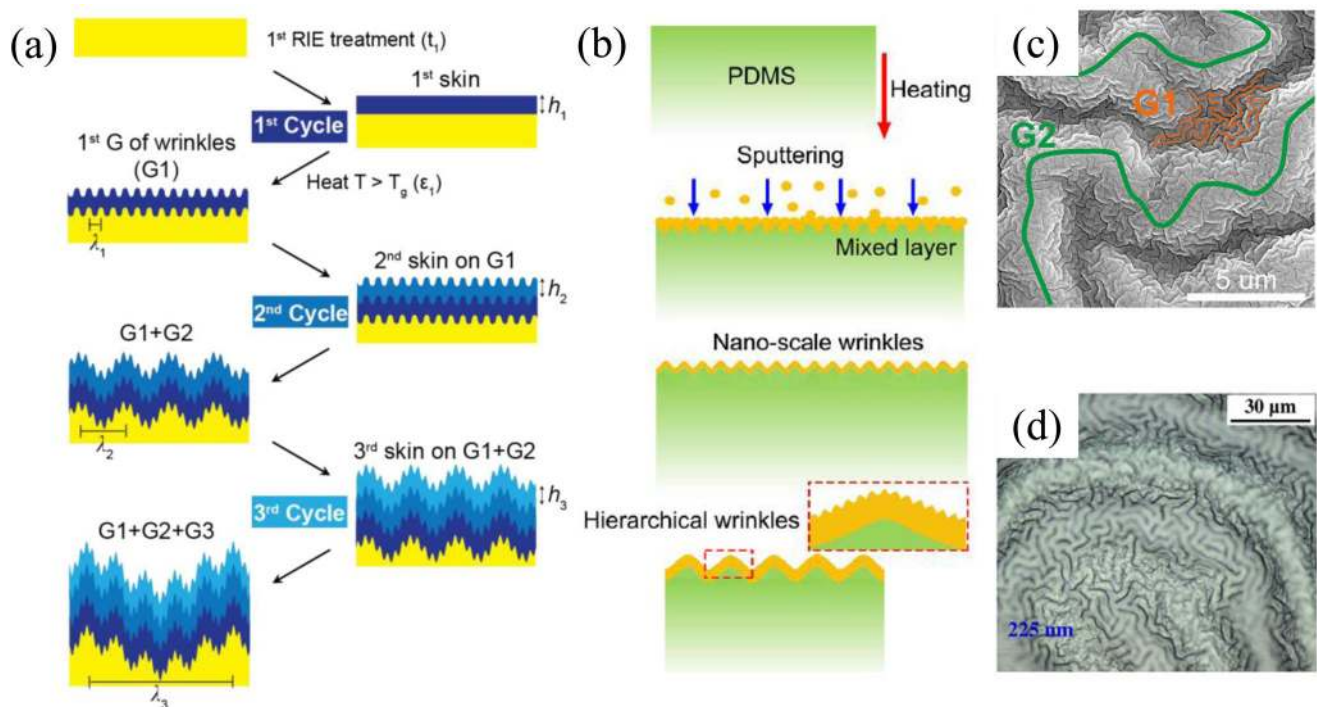
V. OTHER HIERARCHICAL WRINKLES

A. Hierarchical wrinkle by the sequential buckling process

In the film system with gradient elasticity or boundary confinements, hierarchical wrinkling patterns can spontaneously form when the compressive stress exceeds the critical value. In this part, we introduce that the hierarchical wrinkling pattern can also be designed and fabricated by a memory based and sequential strain-release process in a uniform film system. Researchers found that during the release process of a pre-stretched and UV/O treated PDMS skin, when the strain-release rate is relatively slow, the wrinkled skin and stretched substrate form an effective skin that is thicker and stiffer than the initial state. Thus, the followed release leads to much larger wrinkle formation according to Eqs. (2) and (3) and generates nested and hierarchical wrinkling patterns.[97,152] The length scale of these self-similar wrinkles can span five orders of magnitude from a few nanometers to millimeters, which provides the spark for designing artificial hierarchical wrinkling morphologies. Figure 7(a) illustrates the typical procedure for fabricating hierarchical wrinkles.[73] The first generation of wrinkle (G1) is obtained by relieving the strain ε_1 of reactive ion etching (RIE) plasma treated PS film above the glass transition temperature. The wavelength and amplitude of the G1 wrinkle both depend on the initial thickness h_1 under the plasma treatment time t_1 from Eqs. (2) and (3): $\lambda_1 = 2\pi h_1 (\bar{E}_f/3\bar{E}_s)^{1/3}$ and $A_1 = h_1\sqrt{\varepsilon_1/\varepsilon_c - 1}$, where $\bar{E}_f$ and $\bar{E}_s$ are plane strain moduli of the film and substrate, respectively, and ε_c is the critical wrinkle strain of the initial film h_1. Then, a new layer of thickness h_2 grows on the surface of the G1 wrinkle by the plasma treatment with time t_2, and the new layer reserves surface features of the G1 wrinkle. A sequential strain release ε_2 of an effective film of G1 + h_2 produces the G2 wrinkle with a larger wavelength and thus creates hierarchy of wrinkles. The experimental results[73] show that the condition for the formation of a hierarchical wrinkle with two length scales is $h_2 > h_1$. Different from the wavelength $\lambda_{\text{single}} = 2\pi(h_1 + h_2)(\bar{E}_f/3\bar{E}_s)^{1/3}$ of single-generation wrinkle of thickness $h1 + h2$, the wavelength of the G2 wrinkle λ_2 is larger than λ_{single},

$$\lambda_2 = 2\pi g(h_1 + h_2)(\bar{E}_f/3\bar{E}_s)^{1/3}, \quad (12)$$

FIG. 7. (a) Schematic for fabricating hierarchical wrinkles by a sequential strain-release process. An RIE plasma treated PS film would form uniform wrinkling pattern G1 (first generation) after heating treatment. Sequential strain-release process then can produce multi-generational wrinkling pattern (e.g., G1, G2, and G3) with hierarchical wavelength. Reprinted with permission from Lee et al., Nano Lett. **15**, 5624 (2015). Copyright 2015 American Chemical Society. (b) Schematic for intrinsic hierarchical wrinkling on a sputtered metal film on the soft substrate. The metal atoms with high kinetic energy can penetrate into the surface and form a mix layer on the top of PDMS, leading to the formation of intrinsic nano-scale wrinkles. (c) SEM image of hierarchical surface morphology of Al films with thickness of 100 nm (scale bar is 5 μm). G1 and G2 represent nano-scale and mirco-scale wrinkles, respectively. Reprinted with permission from Wu et al., Scr. Mater. **162**, 456 (2019). Copyright 2019 Elsevier Ltd. (e) Optical micrographs of the nested wrinkling pattern of the Mo film with thickness 225 nm on a viscoelastic gel substrate (scale bar is 30 μm). Reprinted with permission from Yu et al., Thin Solid Film **638**, 230 (2017). Copyright 2017 Elsevier Ltd.

where the parameter $g > 1$ introduces the influence of effective skin formed by the G1 wrinkle, which depends on the total film thickness $h_1 + h_2$ and can be defined by experiments. Due to dynamic tunability of the orientation of wrinkles by sequential releasing pre-strain, the sequential wrinkling process has been widely used in controlling the hierarchical surface wrinkling.[99,153,154] The repetition of the sequential process then generates multigenerational hierarchical surface structures with controllable orientations.[73] Figure 1(b) displays a typical image of the hierarchical nanostructure by the sequential wrinkling process. Moreover, the sequential strain-releasing process can act as a powerful tool for designing hierarchical wrinkling patterns by adjusting the film elasticity such as film thickness or the stiffness.

In addition to the critical condition about film thickness, there also exists strain limit to generate morphological hierarchy. It shows that the subsequent released strain ε_2 not only determines the morphological features of the G2 wrinkle, but also modifies the morphology of the G1 wrinkle. For uniaxial sequential compression, the final hierarchical morphology with two generation can be approximately expressed as[41]

$$z(x) = A_L \sin\left(\frac{2\pi x}{\lambda_L}\right) + A_S \sin\left(\frac{2\pi x}{\lambda_S}\right), \quad (13)$$

where subscripts L and S denote the large and small wrinkles, which are generated by G2 and G1 strain-releasing, respectively. The relationship between small wrinkle and releasing strain is expressed by

$$A_s/\lambda_s = \sqrt{\varepsilon_1 - \varepsilon_1\varepsilon_2 - \varepsilon_2^2}/\pi. \quad (14)$$

When there is only one strain-releasing step, means $\varepsilon_2 = 0$, then the small wrinkle degrades into single-generation wrinkle under ε_1 and $A_s, \lambda_s = A_1, \lambda_1$. After releasing strain ε_2 subsequently, however, the G1 wrinkle would weaken with the increase of ε_2 and finally vanish when ε_2 reaches a certain value. So the conditions for producing the hierarchy of the wrinkle is that the film thickness satisfies $h_2 > h_1$,[73] and the sequential release strains satisfy[41]

$$\varepsilon_1 > \varepsilon_2^2/(1 - \varepsilon_2). \quad (15)$$

Otherwise, single-generation wrinkles without hierarchy will be produced in spite of the two-step strain-release process.

Self-similar hierarchical film wrinkles not only possess tunable superhydrophilicity,[73] tunable optical transparency and structural color,[41] and even anisotropic wetting properties,[108] but also can be utilized as cast mold to fabricate monolithic PDMS that inherits three-dimensional hierarchical structures and maintain the excellent wetting properties under repeated stretching.[74] Recently, T. W. Odom's group developed a universal method to fabricate hierarchical three-dimensional surfaces that can be applied to various materials by the sequential wrinkle process,[75] and they reviewed the sequential strain-relief method for preparing self-similar wrinkling surface from thin materials,[76] providing the bottom-up approach for designing hierarchical nanostructures.

For the metal film sputtered on the soft PDMS substrate, there exists intrinsic sequential nested hierarchical wrinkling pattern[129,155] beyond the artificial strain-releasing method. During the sputtering process, the metal atoms with high kinetic energy can penetrate into the surface and form a mix layer upon PDMS substrate.[156–158] The penetration of the metal atoms leads to an expansion of the surface layer and generates compressive stress in the mix layer. When the compressive stress accumulates to the critical wrinkling stress during the sputtering process, the first wrinkle forms to release compressive stress in the sputtered metal film. After film deposition, the second wrinkle is generated by thermal mismatch stress between the film and the substrate whose wavelength is much larger than the first intrinsic wrinkle, as shown in Figs. 7(b)–7(d). Because the first wrinkle appears at a very early stage of the sputtering process and origins from the mix layer expansion, its wavelength and amplitude are found independent of film thickness and remains unchanged during the whole process. While the wavelength and amplitude of the second wrinkle still obey the proportional relationship between thickness, which provides opportunities to design and prepare hierarchical wrinkles in the metal film on the soft substrate.

B. Hierarchical wrinkles guided by templates

Hierarchical wrinkling structures can also be obtained by a template-guide method.[38,159–163] For example, silane treated nanoporous anodic aluminum oxide is used as a template to prepare a PDMS film with various nanopillars on its surface, and the wrinkle of the pre-patterned PDMS leads to the hierarchical surface as shown in Fig. 8.[38] Besides the shape template, glassy nematic coatings can provide a template of stress distribution by regulating the period and orientation of director alignments. Multiscale photoswitchable topographies that contain a wavelength scale and a director distribution period scale can be designed on the soft substrate.[163] The highly oriented PDMS wrinkled surface with a tunable wavelength and amplitude can also act as a suitable template by itself. By a multistep process of conformal contact between the wrinkled template and complaint PDMS with a top layer of the PS film, complex hierarchical wrinkling patterns form on the PS-PDMS substrate.[160] There is another strategy that a hierarchical nanostructure can be obtained by plasma ashing the film of polyelectrolyte multilayer with metallic Ag nanoparticles.[159] Recently, researchers also focus on hierarchical wrinkling on the elastomeric spheres,[164] in which the first order wrinkle with a length scale of a few micrometers results from the elastomer sphere shrinking as solvent evaporates, and the second order wrinkle with a few hundred nanometers results from Grinfeld surface instability.[165,166]

VI. APPLICATIONS OF HIERARCHICAL WRINKLES

Surface wrinkling has acted as a platform to measure thin film properties for years, like the modulus and thickness measurement according to the relationship between wrinkling morphology and elastic modulus,[4,6,167] to investigate the polymer dynamic properties[8] and to control the surface properties.[35] In virtue of the stretchability, the wrinkled surfaces are also used in stretchable functional skins.[32–34] When the chemical reaction and the light responsive effect are considered in film wrinkling, then reversible wrinkling patterns with fluorescence and dynamic optical behaviors are
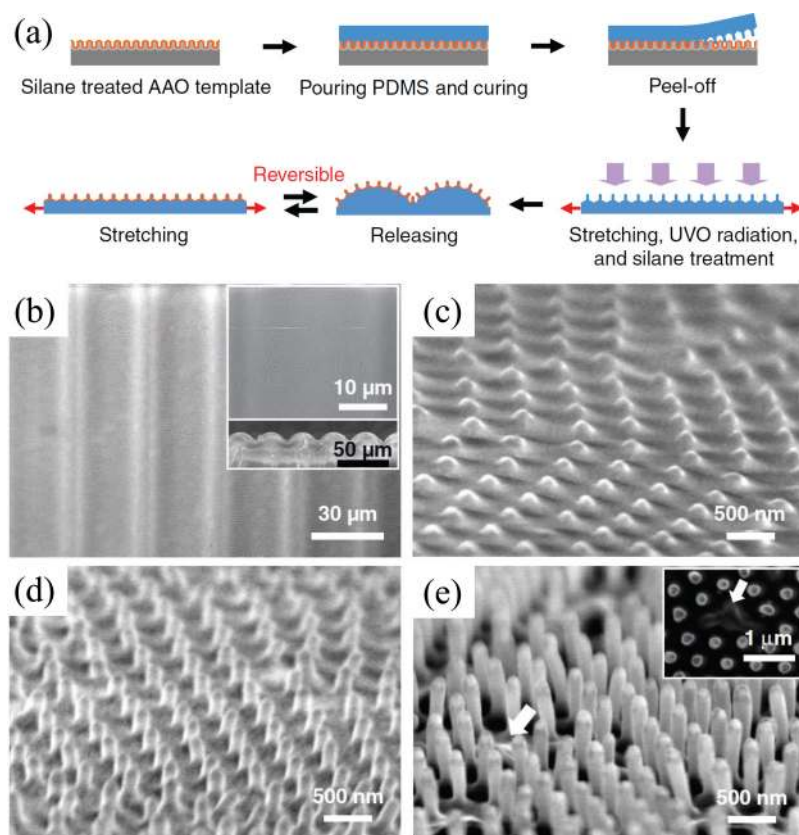
FIG. 8. Scheme and SEM images of the fabricating hierarchical surface structure from various pre-patterned PDMS films, respectively. Reprinted with permission from Lee *et al.*, Adv. Mater. **22**, 5013 (2010). Copyright 2010 Wiley & Sons, Ltd.

introduced.[168–170] Recently, surface wrinkling is utilized in antifouling from a biophysics-inspired mechanism, in which the generated biomimetic surface topography can either influence the attachment probability of biofouling or drive a release of elastic energy stored in the fouling layer to prevent biofouling.[59,171] For hierarchical wrinkles with either continuously varying wavelength/amplitude or self-similar structures, the unique surface structures improve and broaden the previous application. For example, wavy grooves of the wrinkled surface are widely used in the alignment of colloidal particles.[172–178] By taking advantage of multi-scale grooves of gradient wrinkled surfaces as shown in Fig. 9, the alignment of colloidal particles can be optimized in different particle diameters and wrinkle wavelengths. So gradient wrinkling provides a one-step screening platform for optimal assembly of soft and hard colloidal particles.[179] In the system of 2D materials like graphene sheets, the multiscale hierarchical patterns also show excellent tunable of mechanical properties, that the nanoscopic mechanical stiffness and surface adhesion can be locally regulated while the electrical conductivity remain unchanged.[115] Herein, we briefly outline three typical applications of hierarchical wrinkles.

A. Tunable wetting phenomena

Due to the corrugated surface topography, the wetting properties of the wrinkled surface have been widely investigated in recent years.[35–38,171] For hierarchical wrinkled surface with multi-scale structures and spatial distribution, the wetting properties are tunable and unique.[180] Zhang *et al.* investigated the capability of switchable wetting property by applying strain on the hierarchical wrinkled surface.[181] They proposed that with the decrease in the hierarchy of a multi-scale wavy surface, there exists a transition from superhydrophobicity to hydrophobicity and then to hydrophilicity, which is verified by the experimental result afterwards.[41] By a sequential wrinkling process, tunable lotus-type superhydrophobicity is found on the multi-generation hierarchically wrinkled surface as shown in Fig. 10(a).[73] By treating hierarchical films as molds, monolithic PDMS with a hierarchical surface is prepared. The superhydrophobicity of monolithic PDMS can remain after 1000 cycles of stretching and releasing due to its monolithic nature.[74] Besides isotropic wetting properties, on a one-dimensional self-similar hierarchical wrinkled surface, it is found that there is a contact angle difference between the two directions that are parallel and perpendicular to the wrinkle stripes.[108] The unique phenomenon is due to the competition between orthogonal wrinkles and cracks in contact line pinning.

Nested self-similar wrinkled surfaces show outstanding tunable superhydrophobicity for promising applications such as smart window, antifouling coating, and water-resistant electronics. Meanwhile, for the gradient hierarchical wrinkle with continuously varying wavelength and amplitude, the wetting phenomena
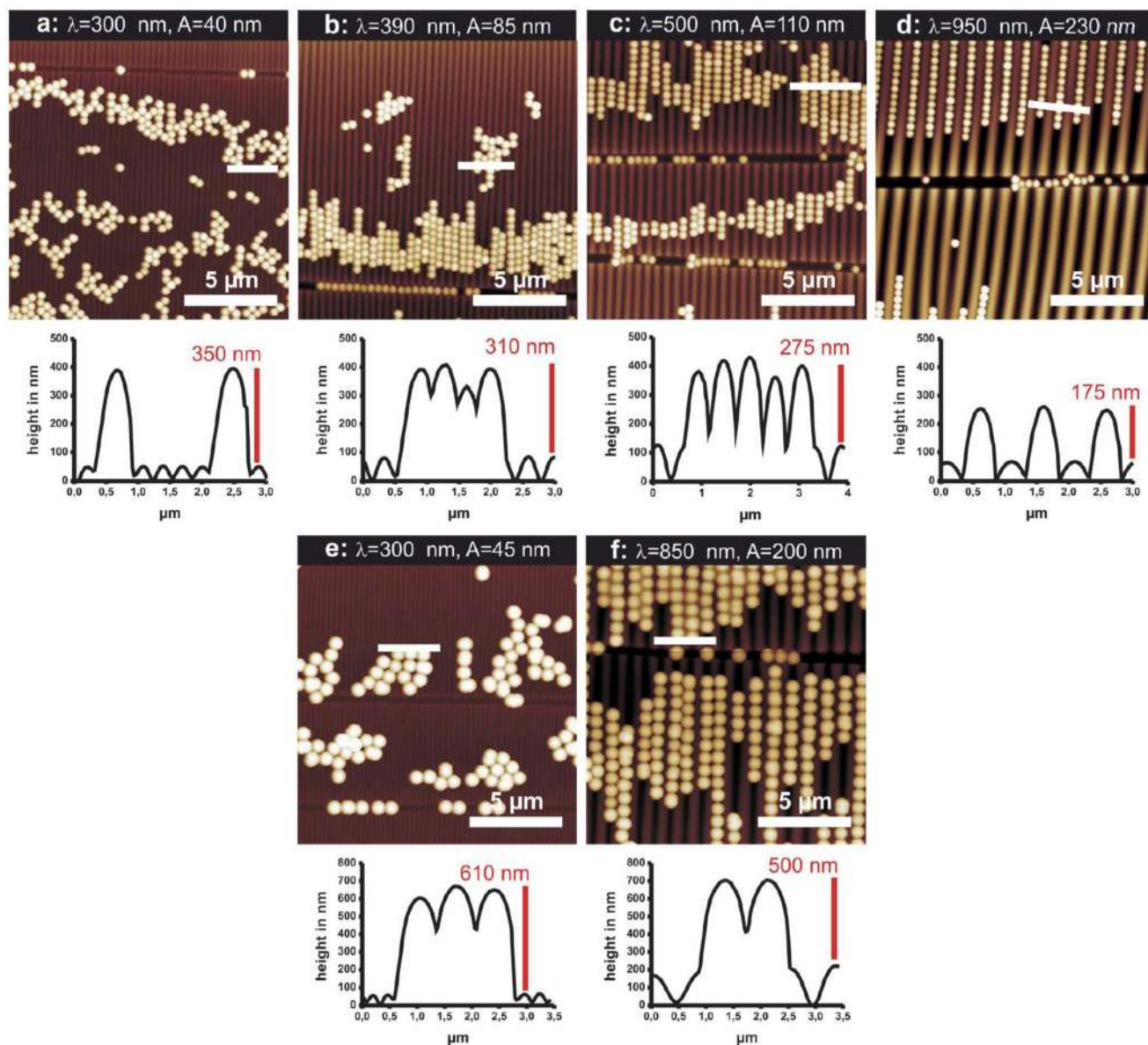
FIG. 9. AFM images and cross sections (correspond to white lines) of silica particles assembled on gradient wrinkled surfaces (scale bar is 5 μm). The red bars indicate the height difference between the particles and the wrinkles. The diameters of particles are 400 nm in (a)–(d) and 700 nm in (e) and (f). Reprinted with permission from Hiltl et al., Nanoscale **4**, 7338 (2012). Copyright 2012 Royal Society of Chemistry.

strongly depend on the local surface structure. When placing a water droplet on a gradient wrinkled surface, there is an obvious contact angle difference between two sides of the droplet along the gradient direction.[182] The surface tension of asymmetrical droplet configuration can drive a movement of water droplet on gradient wrinkling surface from the region of larger wavelength and amplitude to the region with smaller scale, as illustrated in Fig. 10(b).

Self-moving of the droplet on the gradient wrinkled surface provides new opportunities for microfluidic devices.

B. Tunable optical properties

Wrinkled structures have promising optical properties and applications, such as enhancing the light extraction efficiency of
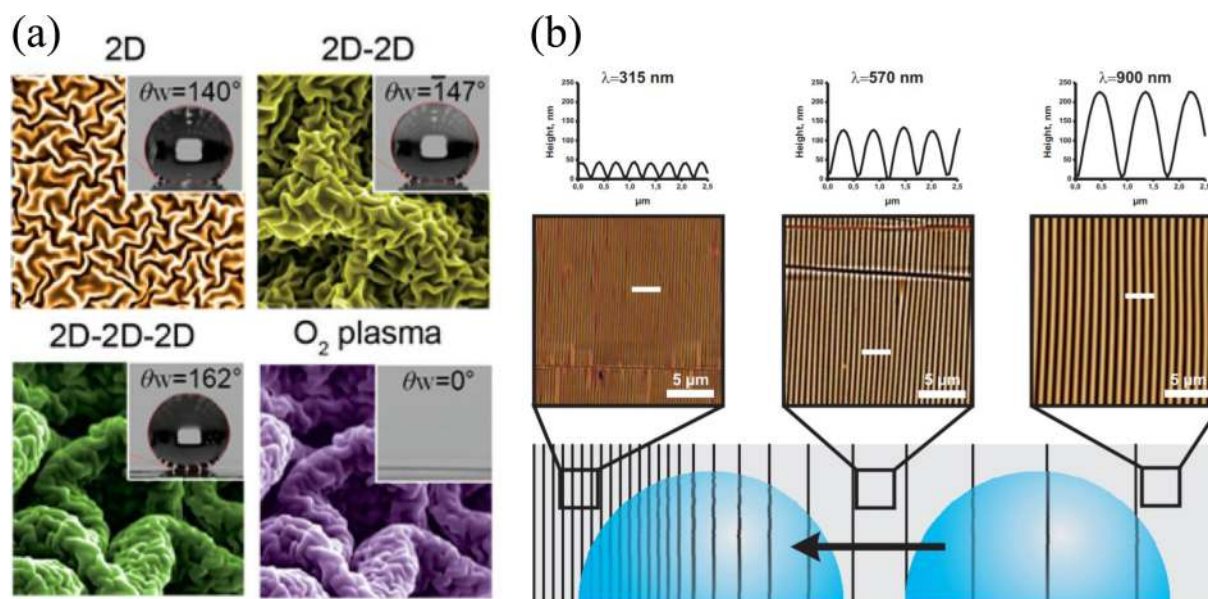
FIG. 10. (a) Tunable superhydrophobicity of self-similar hierarchical wrinkling surfaces. θ_w is the measured static contact angle. Reprinted with permission from Lee *et al.*, Nano Lett. **15**, 5624 (2015). Copyright 2015 American Chemical Society. (b) Sketch of the droplet self-movement on the hierarchical wrinkling surface with a gradient structure. Reprinted with permission from S. Hiltl and A. Böker, Langmuir **32**, 8882 (2016). Copyright 2016 American Chemical Society.
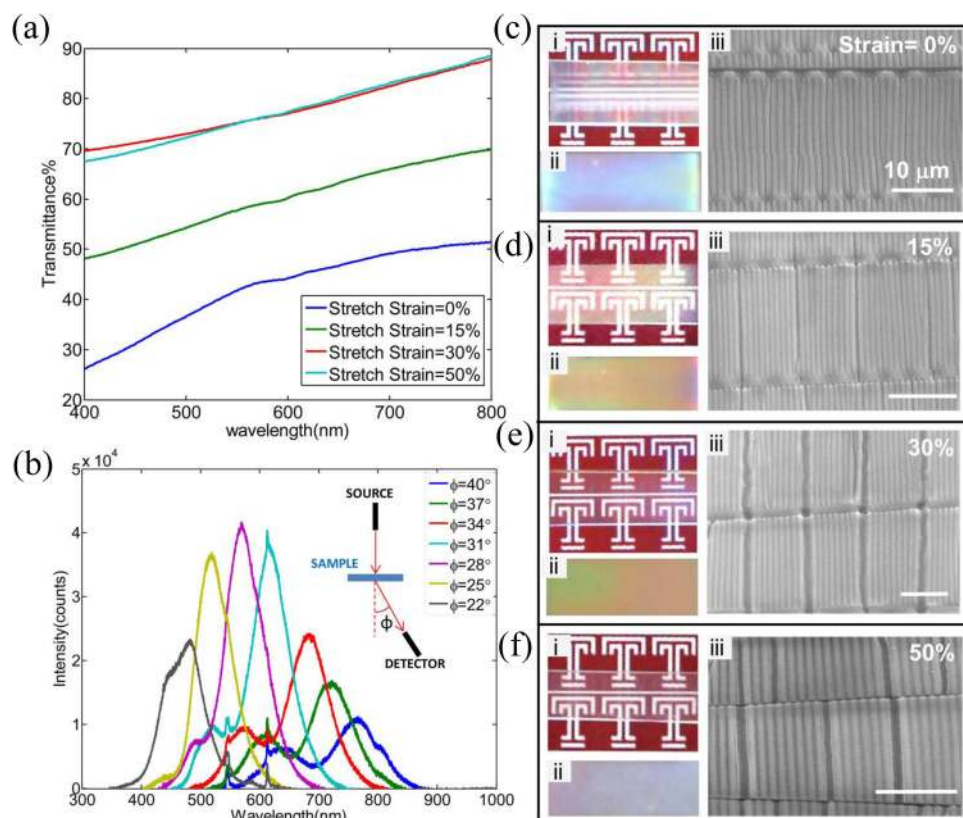

FIG. 11. (a) Tunable transmittance of self-similar hierarchical wrinkled elastomer under different applied stretching strains. (b) Angle-dependent intensity spectrum of the wrinkled elastomer. (c)–(f) Optical images of the transmittance and structure color of hierarchical wrinkles with different applied strains and surface structures. Reprinted with permission from Lin *et al.*, ACS Appl. Mater. Interfaces **9**, 26510 (2017). Copyright 2017 American Chemical Society.

OLED devices due to the random corrugation,[45] preparing optical gratings with various reflected light,[48] and dynamically tuning the transmittance by stretching, heating, and moisturizing.[168,169,183–185] For hierarchical wrinkles prepared by a template-guided method or sequential buckling process, the optical properties strongly rely on the surface structure and can be easily tuned by applied sequential stretching strains.[38,41] Figure 11(a) shows the transmittance of hierarchical wrinkled PDMS increases with the increase in wrinkle wavelength and applied stretch strains, and Fig. 11(b) shows the intensity spectrum at different angles. The results in Figs. 11(c)–11(f) demonstrate that with the increase in applied stretch strain, the hierarchical wrinkled elastomer switches from opaque to translucent state and finally to almost transparent at 30% stretch strain, which means that the optical properties can be easily tuned by the applied strain. Meanwhile, during the stretching process, the elastomer maintains its angle-dependent structure color. The tunability of optical properties of hierarchical wrinkles origins from self-similar structures, in which the applied stretch strain can conveniently change the length scale ratio between first and second wrinkles, and is expected to be applied in the prospective smart widows or optical functional coatings.

C. Tunable platform for cell contact guidance

The wrinkled surface has been widely treated as the platform of cell to investigate the morphology, adhesion, immigration, motility, or proliferation of a cell tissue.[186–190] For hierarchical wrinkles, researchers have found that the shape, orientation, and migration of the cell on the substrate depends on the local surface structure and anisotropy. For instance, the axial ratio of cell in Fig. 12 shows apparent difference on a gradient wrinkled surface, in which the axial ratio in the region with a small wavelength is much larger than that in the region with a large wavelength. Besides, the cell migration trajectory is also distinguishing in different regions of the hierarchical wrinkled surface.[191] To design and guide the cell mechanosensitivity, hierarchical wrinkling patterns are employed as the substrate for fibroblasts. The filopodia attachment is found to be preferentially driven by the topographic features.[128] As for the
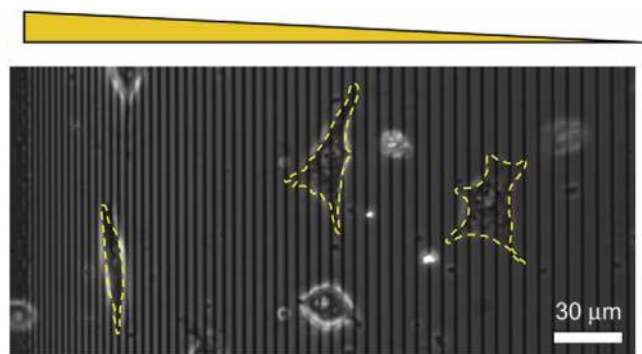
FIG. 12. The different morphologies of fibroblasts on the gradient-corrugated surface. Reprinted with permission from Kim *et al.*, Biomaterials **30**, 5433 (2009). Copyright 2009 Elsevier Ltd.

functional cell differentiation, the gradient roughness surface shows promising potential to modulate the osteogenic differentiation from the stem cell,[192] and the gradient surface can be feasibly prepared using hierarchical wrinkling by elasticity gradient or sequential wrinkling. Compared to a couple of individual uniform wrinkled surface samples, the hierarchical wrinkling pattern provides more surface feature characteristics simultaneously with fewer experiments, which can be used for the high-throughput test platform for cell contact guidance.[112]

VII. CONCLUSIONS

In conclusion, we have reviewed the formation mechanism and corresponding experimental progress of hierarchical wrinkling in elasticity gradient systems, which involve the thickness or modulus gradient. The effects of diffusion and visco-elasticity are also considered as the inducer of elasticity gradient. The boundary confinement provides an alternative physical mechanism to create hierarchical wrinkling near the film edges. Besides, other techniques to prepare a hierarchical wrinkle pattern are introduced, such as the sequential wrinkling process, the template-guide method, and the intrinsic wrinkles during the sputtering process. Hierarchical wrinkling patterns not only inherit the advantages of a general wrinkled surface like outstanding surface properties and stretchability but also can improve the previous applications and show unique characteristics. The wetting and optical properties can be conventionally tuned by changing the hierarchy of wrinkling patterns. In addition, the hierarchical wrinkled surfaces provide an efficient and high-throughput platform for the colloidal particle alignment and cell contact guidance in virtue of the multiscale wavy morphologies, respectively. Hierarchical wrinkling patterns have shown new perspectives in tunable morphologically related applications; however, some challenges still exist. For example, current methods to fabricate hierarchical wrinkles based on wrinkling in the elasticity gradient system only provide the intrinsic wrinkling pattern that strongly depends on its nature. Besides, although the bottom-up sequential wrinkling process can well tune the hierarchy of the surface structure, the wrinkling patterns are lack of spatial variety. Thus, how to fabricate programmable hierarchical wrinkling morphologies feasibly in film–substrate system and 2D materials with or without elasticity gradient still needs to explore. A broad prospect in the functional surface is expected by solving this problem.

ACKNOWLEDGMENTS

REFERENCES

[1]E. Cerda and L. Mahadevan, Phys. Rev. Lett. **90**, 074302 (2003).
[2]B. Li, Y.-P. Cao, X.-Q. Feng, and H. Gao, Soft Matter **8**, 5728 (2012).

[3]S. Deng and V. Berry, Mater. Today **19**, 197 (2016).

[4]C. M. Stafford, C. Harrison, K. L. Beers, A. Karim, E. J. Amis, M. R. VanLandingham, H.-C. Kim, W. Volksen, R. D. Miller, and E. E. Simonyi, Nat. Mater. **3**, 545 (2004).

[5]C. M. Stafford, B. D. Vogt, C. Harrison, D. Julthongpiput, and R. Huang, Macromolecules **39**, 5095 (2006).

[6]E. A. Wilder, S. Guo, S. Lin-Gibson, M. J. Fasolka, and C. M. Stafford, Macromolecules **39**, 4138 (2006).

[7]H. Huang, J. Y. Chung, A. J. Nolte, and C. M. Stafford, Chem. Mater. **19**, 6555 (2007).

[8]E. P. Chan, K. A. Page, S. H. Im, D. L. Patton, R. Huang, and C. M. Stafford, Soft Matter **5**, 4638 (2009).

[9]J. Y. Chung, T. Q. Chastek, M. J. Fasolka, H. W. Ro, and C. M. Stafford, ACS Nano **3**, 844 (2009).

[10]J. Y. Chung, A. J. Nolte, and C. M. Stafford, Adv. Mater. **21**, 1358 (2009).

[11]D. Vella, J. Bico, A. Boudaoud, B. Roman, and P. M. Reis, Proc. Natl. Acad. Sci. U.S.A. **106**, 10901 (2009).

[12]J. E. Longley and M. K. Chaudhury, Macromolecules **43**, 6800 (2010).

[13]E. P. Chan, S. Kundu, Q. Lin, and C. M. Stafford, ACS Appl. Mater. Interfaces **3**, 331 (2011).

[14]J. Y. Chung, J.-H. Lee, K. L. Beers, and C. M. Stafford, Nano Lett. **11**, 3361 (2011).

[15]J. Y. Chung, A. J. Nolte, and C. M. Stafford, Adv. Mater. **23**, 349 (2011).

[16]G. L. Ferretti, M. Nania, O. K. Matar, and J. T. Cabral, Langmuir **32**, 2199 (2016).

[17]S. P. Lacour, S. Wagner, Z. Huang, and Z. Suo, Appl. Phys. Lett. **82**, 2404 (2003).

[18]S. P. Lacour, J. Jones, S. Wagner, L. Teng, and S. Zhigang, Proc. IEEE **93**, 1459 (2005).

[19]D.-Y. Khang, H. Jiang, Y. Huang, and J. A. Rogers, Science **311**, 208 (2006).

[20]W. M. Choi, J. Song, D.-Y. Khang, H. Jiang, Y. Y. Huang, and J. A. Rogers, Nano Lett. **7**, 1655 (2007).

[21]D.-H. Kim, J.-H. Ahn, W. M. Choi, H.-S. Kim, T.-H. Kim, J. Song, Y. Y. Huang, Z. Liu, C. Lu, and J. A. Rogers, Science **320**, 507 (2008).

[22]D.-Y. Khang, J. A. Rogers, and H. H. Lee, Adv. Funct. Mater. **19**, 1526 (2009).

[23]J. A. Rogers, T. Someya, and Y. Huang, Science **327**, 1603 (2010).

[24]Z. Niu, H. Dong, B. Zhu, J. Li, H. H. Hng, W. Zhou, X. Chen, and S. Xie, Adv. Mater. **25**, 1058 (2013).

[25]Y. Ma, K.-I. Jang, L. Wang, H. N. Jung, J. W. Kwak, Y. Xue, H. Chen, Y. Yang, D. Shi, X. Feng, J. A. Rogers, and Y. Huang, Adv. Funct. Mater. **26**, 5345 (2016).

[26]H. E. Jeong, M. K. Kwak, and K. Y. Suh, Langmuir **26**, 2223 (2010).

[27]D. J. Lipomi, B. C.-K. Tee, M. Vosgueritchian, and Z. Bao, Adv. Mater. **23**, 1771 (2011).

[28]M. Melzer, G. Lin, D. Makarov, and O. G. Schmidt, Adv. Mater. **24**, 6468 (2012).

[29]N. Münzenrieder, G. Cantarella, C. Vogt, L. Petti, L. Büthe, G. A. Salvatore, Y. Fang, R. Andri, Y. Lam, R. Libanori, D. Widner, A. R. Studart, and G. Tröster, Adv. Electron. Mater. **1**, 1400038 (2015).

[30]M. Melzer, D. Karnaushenko, G. Lin, S. Baunack, D. Makarov, and O. G. Schmidt, Adv. Mater. **27**, 1333 (2015).

[31]H. Li, Q. Zhan, Y. Liu, L. Liu, H. Yang, Z. Zuo, T. Shang, B. Wang, and R.-W. Li, ACS Nano **10**, 4403 (2016).

[32]J. Mu, C. Hou, G. Wang, X. Wang, Q. Zhang, Y. Li, H. Wang, and M. Zhu, Adv. Mater. **28**, 9491 (2016).

[33]P.-Y. Chen, M. Zhang, M. Liu, I. Y. Wong, and R. H. Hurt, ACS Nano **12**, 234 (2018).

[34]T.-H. Chang, Y. Tian, D. L. Y. Wee, H. Ren, and P.-Y. Chen, Small **14**, 1800596 (2018).

[35]J. Y. Chung, J. P. Youngblood, and C. M. Stafford, Soft Matter **3**, 1163 (2007).

[36]E. P. Chan, E. J. Smith, R. C. Hayward, and A. J. Crosby, Adv. Mater. **20**, 711 (2008).

[37]P.-C. Lin and S. Yang, Soft Matter **5**, 1011 (2009).

[38]S. G. Lee, D. Y. Lee, H. S. Lim, D. H. Lee, S. Lee, and K. Cho, Adv. Mater. **22**, 5013 (2010).

[39]S. Yang, K. Khare, and P.-C. Lin, Adv. Funct. Mater. **20**, 2550 (2010).

[40]J. Zang, S. Ryu, N. Pugno, Q. Wang, Q. Tu, M. J. Buehler, and X. Zhao, Nat. Mater. **12**, 321 (2013).

[41]G. Lin, P. Chandrasekaran, C. Lv, Q. Zhang, Y. Tang, L. Han, and J. Yin, ACS Appl. Mater. Interfaces **9**, 26510 (2017).

[42]D. Rhee, W.-K. Lee, and T. W. Odom, Angew. Chem. Int. Ed. **56**, 6523 (2017).

[43]X. Jiang, T. Shuichi, Q. Xiangping, O. Emanuele, W. Hongkai, B. Ned, L. Philip, E. I. Donald, and M. W. George, Langmuir **18**, 3273 (2002).

[44]C. Harrison, C. M. Stafford, W. Zhang, and A. Karim, Appl. Phys. Lett. **85**, 4016 (2004).

[45]W. H. Koo, S. M. Jeong, F. Araoka, K. Ishikawa, S. Nishimura, T. Toyooka, and H. Takezoe, Nat. Photonics **4**, 222 (2010).

[46]C. Yu, K. O'Brien, Y.-H. Zhang, H. Yu, and H. Jiang, Appl. Phys. Lett. **96**, 041111 (2010).

[47]S. F. Ahmed, G.-H. Rho, K.-R. Lee, A. Vaziri, and M.-W. Moon, Soft Matter **6**, 5709 (2010).

[48]P. J. Yoo, Electron. Mater. Lett. **7**, 17 (2011).

[49]J. B. Kim, P. Kim, N. C. Pégard, S. J. Oh, C. R. Kagan, J. W. Fleischer, H. A. Stone, and Y.-L. Loo, Nat. Photonics **6**, 327 (2012).

[50]P. Kim, Y. Hu, J. Alvarenga, M. Kolle, Z. Suo, and J. Aizenberg, Adv. Opt. Mater. **1**, 381 (2013).

[51]J. Moon, E. Kim, S. K. Park, K. Lee, J.-W. Shin, D.-H. Cho, J. Lee, C. W. Joo, N. S. Cho, J.-H. Han, B.-G. Yu, S. Yoo, and J.-I. Lee, Org. Electron. **26**, 273 (2015).

[52]D. Yin, J. Feng, R. Ma, X. Zhang, Y. Liu, T. Yang, and H. Sun, J. Lightwave Technol. **33**, 3327 (2015).

[53]S. K. Park, Y.-J. Kwark, S. Nam, S. Park, B. Park, S. Yun, J. Moon, J.-I. Lee, B. Yu, and K.-U. Kyung, Polymer **99**, 447 (2016).

[54]J. M. Taylor, C. Argyropoulos, and S. A. Morin, Adv. Mater. **28**, 2595 (2016).

[55]X. Cheng, L. Miao, Z. Su, H. Chen, Y. Song, X. Chen, and H. Zhang, Microsyst. Nanoeng. **3**, 16074 (2017).

[56]E.-H. Ko, H.-J. Kim, S.-M. Lee, T.-W. Kim, and H.-K. Kim, Sci. Rep. **7**, 46739 (2017).

[57]B. Jiang, L. Liu, Z. Gao, and W. Wang, Adv. Opt. Mater. **6**, 1800195 (2018).

[58]K. Efimenko, J. Finlay, M. E. Callow, J. A. Callow, and J. Genzer, ACS Appl. Mater. Interfaces **1**, 1031 (2009).

[59]L. Pocivavsek, J. Pugar, R. O'Dea, S.-H. Ye, W. Wagner, E. Tzeng, S. Velankar, and E. Cerda, Nat. Phys. **14**, 948 (2018).

[60]C. S. Ware, T. Smith-Palmer, S. Peppou-Chapman, L. R. J. Scarratt, E. M. Humphries, D. Balzer, and C. Neto, ACS Appl. Mater. Interfaces **10**, 4173 (2018).

[61]P. Fratzl and R. Weinkamer, Prog. Mater. Sci. **52**, 1263 (2007).

[62]K. Liu, X. Yao, and L. Jiang, Chem. Soc. Rev. **39**, 3240 (2010).

[63]H. Yao and H. Gao, J. Mech. Phys. Solids **54**, 1120 (2006).

[64]P. Fratzl, H. Gupta, E. Paschalis, and P. Roschger, J. Mater. Chem. **14**, 2115 (2004).

[65]Y. Oaki and H. Imai, Angew. Chem. Int. Ed. **44**, 6571 (2005).

[66]J. Huang, B. Davidovitch, C. D. Santangelo, T. P. Russell, and N. Menon, Phys. Rev. Lett. **105**, 038302 (2010).

[67]G. Gioia, A. DeSimone, M. Ortiz, and A. M. Cuitiño, Proc. R. Soc. Lond. Ser. A Math. Phys. Eng. Sci. **458**, 1223 (2002).

[68]S. Conti, A. DeSimone, and S. Müller, Comput. Method Appl. Mech. Eng. **194**, 2534 (2005).

[69]H. Vandeparre, M. Piñeirua, F. Brau, B. Roman, J. Bico, C. Gay, W. Bao, C. N. Lau, P. M. Reis, and P. Damman, Phys. Rev. Lett. **106**, 224301 (2011).

[70]H. King, R. D. Schroll, B. Davidovitch, and N. Menon, Proc. Natl. Acad. Sci. U.S.A. **109**, 9716 (2012).

[71]S. Deng and V. Berry, ACS Appl. Mater. Interfaces **8**, 24956 (2016).

[72]S. Yu, Y. Sun, X. Zhang, C. Lu, H. Zhou, and Y. Ni, Phys. Rev. E **99**, 062802 (2019).

[73]W.-K. Lee, C. J. Engel, M. D. Huntington, J. Hu, and T. W. Odom, Nano Lett. **15**, 5624 (2015).

[74]W.-K. Lee, W.-B. Jung, S. R. Nagel, and T. W. Odom, Nano Lett. **16**, 3774 (2016).

[75]W.-B. Jung, K. M. Cho, W.-K. Lee, T. W. Odom, and H.-T. Jung, ACS Appl. Mater. Interfaces **10**, 1347 (2018).

[76]W.-K. Lee and T. W. Odom, ACS Nano **13**, 6170 (2019).

[77]H. G. Allen, *Analysis and Design of Structural Sandwich Panels: The Commonwealth and International Library: Structures and Solid Body Mechanics Division* (Elsevier, 2013).

[78]N. Bowden, S. Brittain, A. G. Evans, J. W. Hutchinson, and G. M. Whitesides, Nature **393**, 146 (1998).

[79]N. Bowden, W. T. S. Huck, K. E. Paul, and G. M. Whitesides, Appl. Phys. Lett. **75**, 2557 (1999).

[80]A. L. Volynskii, S. Bazhenov, O. V. Lebedeva, and N. F. Bakeev, J. Mater. Sci. **35**, 547 (2000).

[81]J. Groenewold, Physica A **298**, 32 (2001).

[82]R. Huang and Z. Suo, J. Appl. Phys. **91**, 1135 (2002).

[83]E. Cerda, K. Ravi-Chandar, and L. Mahadevan, Nature **419**, 579 (2002).

[84]X. Chen and J. W. Hutchinson, J. Appl. Mech. **71**, 597 (2004).

[85]R. Huang, J. Mech. Phys. Solids **53**, 63 (2005).

[86]Z. Huang, W. Hong, and Z. Suo, Phys. Rev. E **70**, 030601 (2004).

[87]Z. Y. Huang, W. Hong, and Z. Suo, J. Mech. Phys. Solids **53**, 2101 (2005).

[88]B. Audoly and A. Boudaoud, J. Mech. Phys. Solids **56**, 2401 (2008).

[89]S. Cai, D. Breid, A. J. Crosby, Z. Suo, and J. W. Hutchinson, J. Mech. Phys. Solids **59**, 1094 (2011).

[90]J. Yin and X. Chen, Philos. Mag. Lett. **90**, 423 (2010).

[91]Y. Ni, D. Yang, and L. He, Phys. Rev. E **86**, 031604 (2012).

[92]J. W. Cahn and J. E. Hilliard, J. Chem. Phys. **28**, 258 (1958).

[93]J. Zhao, X. Guo, and L. Lu, Appl. Math. Mech. **38**, 617 (2017).

[94]S. Yu, Y. Ni, L. He, and Q.-L. Ye, ACS Appl. Mater. Interfaces **7**, 5160 (2015).

[95]D. B. H. Chua, H. T. Ng, and S. F. Y. Li, Appl. Phys. Lett. **76**, 721 (2000).

[96]W. T. S. Huck, N. Bowden, P. Onck, T. Pardoen, J. W. Hutchinson, and G. M. Whitesides, Langmuir **16**, 3497 (2000).

[97]K. Efimenko, M. Rackaitis, E. Manias, A. Vaziri, L. Mahadevan, and J. Genzer, Nat. Mater. **4**, 293 (2005).

[98]E. P. Chan and A. J. Crosby, Adv. Mater. **18**, 3238 (2006).

[99]P.-C. Lin and S. Yang, Appl. Phys. Lett. **90**, 241903 (2007).

[100]M. Guvendiren, S. Yang, and J. A. Burdick, Adv. Funct. Mater. **19**, 3038 (2009).

[101]D. Chandra and A. J. Crosby, Adv. Mater. **23**, 3441 (2011).

[102]D. Breid and A. J. Crosby, Soft Matter **7**, 4490 (2011).

[103]S. J. Ma, S. J. Mannino, N. J. Wagner, and C. J. Kloxin, ACS Macro Lett. **2**, 474 (2013).

[104]F. A. Bayley, J. L. Liao, P. N. Stavrinou, A. Chiche, and J. T. Cabral, Soft Matter **10**, 1155 (2014).

[105]Q. Li, X. Han, J. Hou, J. Yin, S. Jiang, and C. Lu, J. Phys. Chem. B **119**, 13450 (2015).

[106]M. Nania, O. K. Matar, and J. T. Cabral, Soft Matter **11**, 3067 (2015).

[107]Z.-J. Zhao, J.-H. Yang, X. Li, and S.-H. Park, Mater. Lett. **164**, 23 (2016).

[108]G. Lin, Q. Zhang, C. Lv, Y. Tang, and J. Yin, Soft Matter **14**, 1517 (2018).

[109]M. Ouyang, C. Yuan, R. J. Muisener, A. Boulares, and J. T. Koberstein, Chem. Mater. **12**, 1591 (2000).

[110]K. Efimenko, W. E. Wallace, and J. Genzer, J. Colloid Interface Sci. **254**, 306 (2002).

[111]H. Hillborg, N. Tomczak, A. Olàh, H. Schönherr, and G. J. Vancso, Langmuir **20**, 785 (2004).

[112]Q. Zhou, P. T. Kühn, T. Huisman, E. Nieboer, C. van Zwol, T. G. van Kooten, and P. van Rijn, Sci. Rep. **5**, 16240 (2015).

[113]H. Li, B. Sheng, H. Wu, Y. Huang, D. Zhang, and S. Zhuang, Materials **11**, 1571 (2018).

[114]J. Rodríguez-Hernández and A. del Campo, J. Appl. Polym. Sci. **132**, 41863 (2015).

[115]W.-K. Lee, J. Kang, K.-S. Chen, C. J. Engel, W.-B. Jung, D. Rhee, M. C. Hersam, and T. W. Odom, Nano Lett. **16**, 7121 (2016).

[116]J. Lim, S.-J. Choi, and P. Kim, Adv. Mater. Interfaces **5**, 1701109 (2018).

[117]J. C. Meredith, A. P. Smith, A. Karim, and E. J. Amis, Macromolecules **33**, 9747 (2000).

[118]G. Miquelard-Garnier, A. B. Croll, C. S. Davis, and A. J. Crosby, Soft Matter **6**, 5789 (2010).

[119]A. E. Schedl, C. Neuber, A. Fery, and H.-W. Schmidt, Langmuir **34**, 14249 (2018).

[120]K. U. Claussen, T. Scheibel, H.-W. Schmidt, and R. Giesa, Macromol. Mater. Eng. **297**, 938 (2012).

[121]K. U. Claussen, M. Tebbe, R. Giesa, A. Schweikart, A. Fery, and H.-W. Schmidt, RSC Adv. **2**, 10185 (2012).

[122]B. A. Glatz, M. Tebbe, B. Kaoui, R. Aichele, C. Kuttner, A. E. Schedl, H.-W. Schmidt, W. Zimmermann, and A. Fery, Soft Matter **11**, 3332 (2015).

[123]I. D. Johnston, D. K. McCluskey, C. K. L. Tan, and M. C. Tracey, J. Micromech. Microeng. **24**, 035017 (2014).

[124]S. Roy, N. Bhandaru, R. Das, G. Harikrishnan, and R. Mukherjee, ACS Appl. Mater. Interfaces **6**, 6579 (2014).

[125]S. Yu, Y. Sun, Y. Ni, X. Zhang, and H. Zhou, ACS Appl. Mater. Interfaces **8**, 5706 (2016).

[126]K. Li, J. Wang, B. Shao, J. Xiao, H. Zhou, and S. Yu, Thin Solid Films **654**, 100 (2018).

[127]V. Parihar, S. Bandyopadhyay, S. Das, R. Mukherjee, S. Chakraborty, and S. Dasgupta, Soft Matter **14**, 7034 (2018).

[128]H. Vandeparre, S. Gabriele, F. Brau, C. Gay, K. K. Parker, and P. Damman, Soft Matter **6**, 5751 (2010).

[129]S.-J. Yu, Y.-P. Du, Y.-D. Sun, Q.-L. Ye, and H. Zhou, Thin Solid Films **638**, 230 (2017).

[130]H. Vandeparre and P. Damman, Phys. Rev. Lett. **101**, 124301 (2008).

[131]H. Vandeparre, J. Léopoldès, C. Poulard, S. Desprez, G. Derue, C. Gay, and P. Damman, Phys. Rev. Lett. **99**, 188302 (2007).

[132]H. Vandeparre, S. Desbief, R. Lazzaroni, C. Gay, and P. Damman, Soft Matter **7**, 6878 (2011).

[133]S. H. Im and R. Huang, J. Appl. Mech. **72**, 955 (2005).

[134]R. Huang and S. H. Im, Phys. Rev. E **74**, 026214 (2006).

[135]S. H. Im and R. Huang, J. Mech. Phys. Solids **56**, 3315 (2008).

[136]A. Das, A. Banerji, and R. Mukherjee, ACS Appl. Mater. Interfaces **9**, 23255 (2017).

[137]Y. Ni, L. He, and Q. Liu, Phys. Rev. E **84**, 051604 (2011).

[138]J. W. Hutchinson, M. D. Thouless, and E. G. Liniger, Acta Metall. Mater. **40**, 295 (1992).

[139]M. W. Moon, H. M. Jensen, J. W. Hutchinson, K. H. Oh, and A. G. Evans, J. Mech. Phys. Solids **50**, 2355 (2002).

[140]G. Parry, A. Cimetière, C. Coupeau, J. Colin, and J. Grilhé, Phys. Rev. E **74**, 066601 (2006).

[141]A. A. Abdallah, D. Kozodaev, P. C. P. Bouten, J. M. J. den Toonder, U. S. Schubert, and G. de With, Thin Solid Films **503**, 167 (2006).

[142]J.-Y. Faou, G. Parry, S. Grachev, and E. Barthel, Phys. Rev. Lett. **108**, 116102 (2012).

[143]K. Pan, Y. Ni, L. He, and R. Huang, Int. J. Solids Struct. **51**, 3715 (2014).

[144]A. Ruffini, J. Durinck, J. Colin, C. Coupeau, and J. Grilhé, Acta Mater. **60**, 1259 (2012).

[145]A. Ruffini, J. Durinck, J. Colin, C. Coupeau, and J. Grilhé, Scr. Mater. **67**, 157 (2012).

[146]K. Pan, Y. Ni, and L. He, Phys. Rev. E **88**, 062405 (2013).

[147]S.-C. Li, S.-J. Yu, L. He, and Y. Ni, J. Mech. Phys. Solids **112**, 637 (2018).

[148]S.-J. Yu, Y.-J. Zhang, H. Zhou, M.-G. Chen, X.-F. Zhang, Z.-W. Jiao, and P.-Z. Si, Phys. Rev. E **88**, 042401 (2013).

[149]M. Ortiz and G. Gioia, J. Mech. Phys. Solids **42**, 531 (1994).

[150]W. Jin and P. Sternberg, J. Math. Phys. **42**, 192 (2001).

[151]W. Bao, F. Miao, Z. Chen, H. Zhang, W. Jang, C. Dames, and C. N. Lau, Nat. Nanotechnol. **4**, 562 (2009).

[152]M.-W. Moon and A. Vaziri, Scr. Mater. **60**, 44 (2009).

[153]J. Yin, J. L. Yagüe, D. Eggenspieler, K. K. Gleason, and M. C. Boyce, Adv. Mater. **24**, 5441 (2012).

[154]J. Yin, J. L. Yagüe, M. C. Boyce, and K. K. Gleason, ACS Appl. Mater. Interfaces **6**, 2850 (2014).

[155]K. Wu, H. Z. Yuan, S. J. Li, J. Y. Zhang, G. Liu, and J. Sun, Scr. Mater. **162**, 456 (2019).

[156]P. Slepička, T. Fidler, A. Vasina, and V. Švorčík, Mater. Lett. **79**, 4 (2012).

[157]P. Slepička, P. Juřík, P. Malinský, A. Macková, N. S. Kasálková, and V. Švorčík, Nucl. Instrum. Methods Phys. Res. B **332**, 7 (2014).

[158]P. Juřík, P. Slepička, M. Nagyová, and V. Švorčík, Surf. Coat. Technol. **311**, 344 (2017).

[159]Y. H. Kim, Y. M. Lee, J. Y. Lee, M. J. Ko, and P. J. Yoo, ACS Nano **6**, 1082 (2012).

[160]J. Yin and C. Lu, Soft Matter **8**, 6528 (2012).

[161]P. Goel, S. Kumar, J. Sarkar, and J. P. Singh, ACS Appl. Mater. Interfaces **7**, 8419 (2015).

[162]J. Choi, J. Mun, M. C. Wang, A. Ashraf, S.-W. Kang, and S. Nam, Nano Lett. **17**, 1756 (2017).

[163]W. X. Qian, Y. Ni, and L. H. He, Phys. Rev. E **99**, 052702 (2019).

[164]A. C. Trindade, J. P. Canejo, P. Patrício, P. Brogueira, P. I. Teixeira, and M. H. Godinho, J. Mater. Chem. **22**, 22044 (2012).

[165]M. A. Grinfeld, Akad. Nauk SSSR, Dokl. **290**, 1358 (1986).

[166]J. Berréhar, C. Caroli, C. Lapersonne-Meyer, and M. Schott, Phys. Rev. B **46**, 13487 (1992).

[167]D.-Y. Khang, J. Xiao, C. Kocabas, S. MacLaren, T. Banks, H. Jiang, Y. Y. Huang, and J. A. Rogers, Nano Lett. **8**, 124 (2008).

[168]H. Hou, J. Yin, and X. Jiang, Adv. Mater. **28**, 9126 (2016).

[169]F. Li, H. Hou, J. Yin, and X. Jiang, Sci. Adv. **4**, eaar5762 (2018).

[170]M. Xie, F. Xu, L. Zhang, J. Yin, and X. Jiang, ACS Macro Lett. **7**, 540 (2018).

[171]J. Fu, H. Zhang, Z. Guo, D.-Q. Feng, V. Thiyagarajan, and H. Yao, J. R. Soc. Interface **15**, 20170823 (2018).

[172]S. Hiltl, M.-P. Schürings, A. Balaceanu, V. Mayorga, C. Liedel, A. Pich, and A. Böker, Soft Matter **7**, 8231 (2011).

[173]M. Müller, M. Karg, A. Fortini, T. Hellweg, and A. Fery, Nanoscale **4**, 2491 (2012).

[174]R. Brüx, S. Hiltl, V. Schröder, C. von Essen, and A. Böker, Part. Part. Syst. Charact. **31**, 871 (2014).

[175]H. Endo, Y. Mochizuki, M. Tamura, and T. Kawai, Colloids Surf. A **443**, 576 (2014).

[176]C. Hanske, M. Tebbe, C. Kuttner, V. Bieber, V. V. Tsukruk, M. Chanana, T. A. F. König, and A. Fery, Nano Lett. **14**, 6863 (2014).

[177]P. Wünnemann, M. Noyong, K. Kreuels, R. Brüx, P. Gordiichuk, P. van Rijn, F. A. Plamper, U. Simon, and A. Böker, Macromol. Rapid Commun. **37**, 1446 (2016).

[178]M.-P. Schürings, O. Nevskyi, K. Eliasch, A.-K. Michel, B. Liu, A. Pich, A. Böker, G. Von Plessen, and D. Wöll, Polymers **8**, 413 (2016).

[179]S. Hiltl, J. Oltmanns, and A. Böker, Nanoscale **4**, 7338 (2012).

[180]W.-B. Jung, G.-T. Yun, Y. Kim, M. Kim, and H.-T. Jung, ACS Appl. Mater. Interfaces **11**, 7546 (2019).

[181]Z. Zhang, T. Zhang, Y. W. Zhang, K.-S. Kim, and H. Gao, Langmuir **28**, 2753 (2012).

[182]S. Hiltl and A. Böker, Langmuir **32**, 8882 (2016).

[183]M. Shrestha and G.-K. Lau, Opt. Lett. **41**, 4433 (2016).

[184]Z. Li, Y. Zhai, Y. Wang, G. M. Wendland, X. Yin, and J. Xiao, Adv. Opt. Mater. **5**, 1700425 (2017).

[185]S. Zeng, R. Li, S. G. Freire, V. M. M. Garbellotto, E. Y. Huang, A. T. Smith, C. Hu, W. R. T. Tait, Z. Bian, G. Zheng, D. Zhang, and L. Sun, Adv. Mater. **29**, 1700828 (2017).

[186]A. Schweikart and A. Fery, Microchim. Acta **165**, 249 (2009).

[187]M. Guvendiren and J. A. Burdick, Biomaterials **31**, 6511 (2010).

[188]Z. Zhao, J. Gu, Y. Zhao, Y. Guan, X. X. Zhu, and Y. Zhang, Biomacromolecules **15**, 3306 (2014).

[189]A. Paul, M. Stührenberg, S. Chen, D. Rhee, W. K. Lee, T. W. Odom, S. C. Heilshorn, and A. Enejder, Soft Matter **13**, 5665 (2017).

[190]E. Martinez-Campos, A. Gallardo, N. Lujan, A. Santos-Coquillat, H. Reinecke, A. D. Campo, and J. Rodriguez-Hernandez, ACS Appl. Bio Mater. **2**, 654 (2019).

[191]D.-H. Kim, K. Han, K. Gupta, K. W. Kwon, K.-Y. Suh, and A. Levchenko, Biomaterials **30**, 5433 (2009).

[192]A. B. Faia-Torres, S. Guimond-Lischer, M. Rottmar, M. Charnley, T. Goren, K. Maniura-Weber, N. D. Spencer, R. L. Reis, M. Textor, and N. M. Neves, Biomaterials **35**, 9023 (2014).